Doctor of Philosophy

Human vascular tissue fabrication using the co-culture of vascular cells

The Graduate School of the University of Ulsan

Department of Electrical, Electronic and Computer Engineering

Duong Van Thuy

Human vascular tissue fabrication using the co-culture of vascular cells

Supervisor: Professor Koo, Kyo-in

A Dissertation
Submitted to the Graduate School of the University of Ulsan in Partial
Fulfillment of the Requirements for the Degree of
Doctor of Philosophy

by

Duong Van Thuy

Department of Electrical, Electronic and Computer Engineering

University of Ulsan, South Korea

February 2022

Human vascular tissue fabrication using the co-culture of vascular cells

This certifies that the dissertation of Duong Van Thuy is approved

Committee Chairman:	Dr. Woo, Ji-Hwan
Committee Member:	Dr. Koo, Kyo-in
Committee Member:	Dr. Chee, Young-joon
Committee Member:	Dr. Kim, Sungmin
Committee Member:	Dr. Back, Sung Hoon
Committee Member:	Dr. Cha, Chaenyung

Department of Electrical, Electronic and Computer Engineering

University of Ulsan, South Korea

February 2022

Acknowledgments

First and foremost, I am extremely grateful to my supervisor, Prof. **Kyo-in Koo**, for his invaluable advice, support, and patience during my Ph.D. study. His immense knowledge and plentiful experience have encouraged me in all the time of my academic research and my daily life.

Besides my advisor, I would like to thank the rest of my dissertation committee: Prof. Ji-Hwan Woo, Prof. Young-joon Chee, Prof. Sungmin Kim, Prof. Sung Hoon Back, and Prof. Chaenyung Cha for their encouragement, insightful comments that helped me to further improve my dissertation.

I highly appreciate and show my gratitude to Prof. Sung Hoon Back, Prof. Chaenyung Cha (UNIST) and his students, Mrs. Yeasol Lee, Mr. Sangyeol Lee, Dr. Mi Jeong Kim, Dr. Thao Thi Dang, Mr. 이대영 (Kyungpook National University) for their co-working, training, service, and supporting during my Ph.D.

I would like to thank all the alumni and members of the Medical Device Lab, UoU. It is their kind help and support that made my study and life in Korea a wonderful time.

Finally, I would like to express my gratitude to my parents, my wife, and my big family. Without their tremendous understanding and encouragement in the past few years, it would be impossible for me to complete my study.

Duong Van Thuy

Abstract

Using a microfluidic-based core-shell nozzle, human umbilical vein endothelial cells (HUVECs) and human aortic smooth muscle cells (HASMCs) were coaxially and continuously printed without ultraviolet light. The core material was Type I collagen (3 mg/ml) including HUVECs and a crosslinking reagent (100 mM $CaCl_2$). Simultaneously, a blend of 3 mg/ml type I collagen (25%) and 1.8 percent weight/volume sodium alginate (75%) was used as a shell material around the core. The HUVECs proliferated in the scaffold's core and reorganized themselves into a monolayer along the axial direction while the HASMCs showed more than 90% cell viability in the shell layer. Using an in-house micro connector, fluorescent microparticles were fed through the inner channel of the scaffold with the HUVEC core and HASMC shell. In growth factor-free media, this double-layered scaffold demonstrated more angiogenesis than the scaffold with simply a HUVEC core. Angiogenesis, extracellular matrix secretion, and outer diameter were all altered by the HASMCs in the shell layer. The developed method might be used to produce high-volume vascularized tissue using three-dimensional bioprinting.

Contents

List of Figures

List of Tables

List of Abbreviations

#	Short name	Full name
1	EC	Endothelial cell
2	SMC	Smooth muscle cell
3	ECM	Extracellular matrix
4	3D	Three-dimensional
5	TEVG	Tissue-engineered vascular graft
6	PAD	Peripheral artery disease
7	GelMA	Gelatine methacryloyl
8	PEGOA	Poly(ethylene glycol) acrylate
9	UV	Ultraviolet
10	DECM	Decellularized extracellular matrix
11	HUVEC	Human umbilical vein endothelial cell
12	HASMC	Human aortic smooth muscle cell
13	HF	Human fibroblast
14	NIH/3T3	Mouse fibroblast
15	PDMS	Polydimethylsiloxane
16	$CaCl_2$	Calcium chloride
17	PDGF	Platelet-derived growth factor
18	VEGF	Vascular endothelial growth factor
19	$MgCl_2$	Magnesium chloride
20	NaCl	sodium chloride
21	PBS	Phosphate buffered saline
22	NaOH	Sodium hydroxide
23	DMEM	Dulbecco's Modified Eagle Medium
24	SEM	Scanning electron microscopy
25	DMSO	Dimethyl sulfoxide

26	FBS	Fetal bovine serum
27	RT	Room temperature
28	ID	Inner diameter
29	OD	Outer diameter
30	GF	Growth factor
31	EDTA	Ethylenediaminetetraacetic acid
32	RNA	Ribonucleic acid
33	cDNA	complementary DNA
34	qPCR	quantitative polymerase chain reaction
35	TGF	Transforming growth factor
36	C25-A75	25% collagen + 75% alginate
37	HE	Hematoxylin and eosin
38	HGF	Hepatocyte growth factor
39	BSA	Bovine serum albumin

Chapter 1:
Introduction

1.1 Human vascular system

In the human body, the circulatory system or known as the vascular system comprises vessels that circulate blood to almost entire organs and tissues (Figure 1). Nutrients and oxygen are transported to living cells in order to feed the cells meanwhile metabolic wastes such as nitrogen compounds, carbon dioxide (CO_2), phosphates are carried to the excretory system by the vascular system [1-3]. The vessels of the blood circulatory system have a tubular lumen structure and are categorized into three types [4]: (1) Arteries. Blood vessels contain a thick and strong, muscular middle layer of smooth muscle cells (SMCs) and an interior monolayer of endothelial cells (ECs). Arteries pump oxygenated blood from the heart to the organs and tissues. (2) Veins. Blood vessels are similar to arteries but have a thinner and weaker muscular layer. Veins carry blood from the organs and tissues back into the heart. Unlike arteries, veins contain one-way valves that ensure blood flows in only one direction (3) Capillaries. Permeable blood vessels between arteries and veins that made of a monolayer of endothelial cells that allows to diffusing oxygen, CO_2, nutrients, and other molecular compounds.

Except capillaries, most blood vessels mainly contain three layers (Figure 2) [5, 6]. The tunica intima is the vessel's innermost layer that directly touches the blood. This layer consists of a monolayer of ECs that forms the lumen of the vessel. The middle layer, the tunica media, is predominantly made up of extracellular matrix (ECM), mostly elastin and collagen, as well as circularly-organized SMCs. The ECM permits the vessel to stretch and recoil while the SMCs govern contraction and relaxation. This layer has the ability to change the diameter of the vessel (known as vasodilation and vasoconstriction) [7]. The tunica externa is the outermost layer that mostly consists of ECMs, fibroblasts, loosely collagen fibres, connective components, autonomic nerves, vasa vasorum, and lymphatic vessels. The other layers of the vessel are protected by this layer, which anchors them to the surrounding tissues. Indeed, Bergman *et al.* used

longitudinal and circumferential anatomical observations to empirically show the general structure of human arterioles with a diameter less than 500 micrometres (μm) with three distinct layers [8].

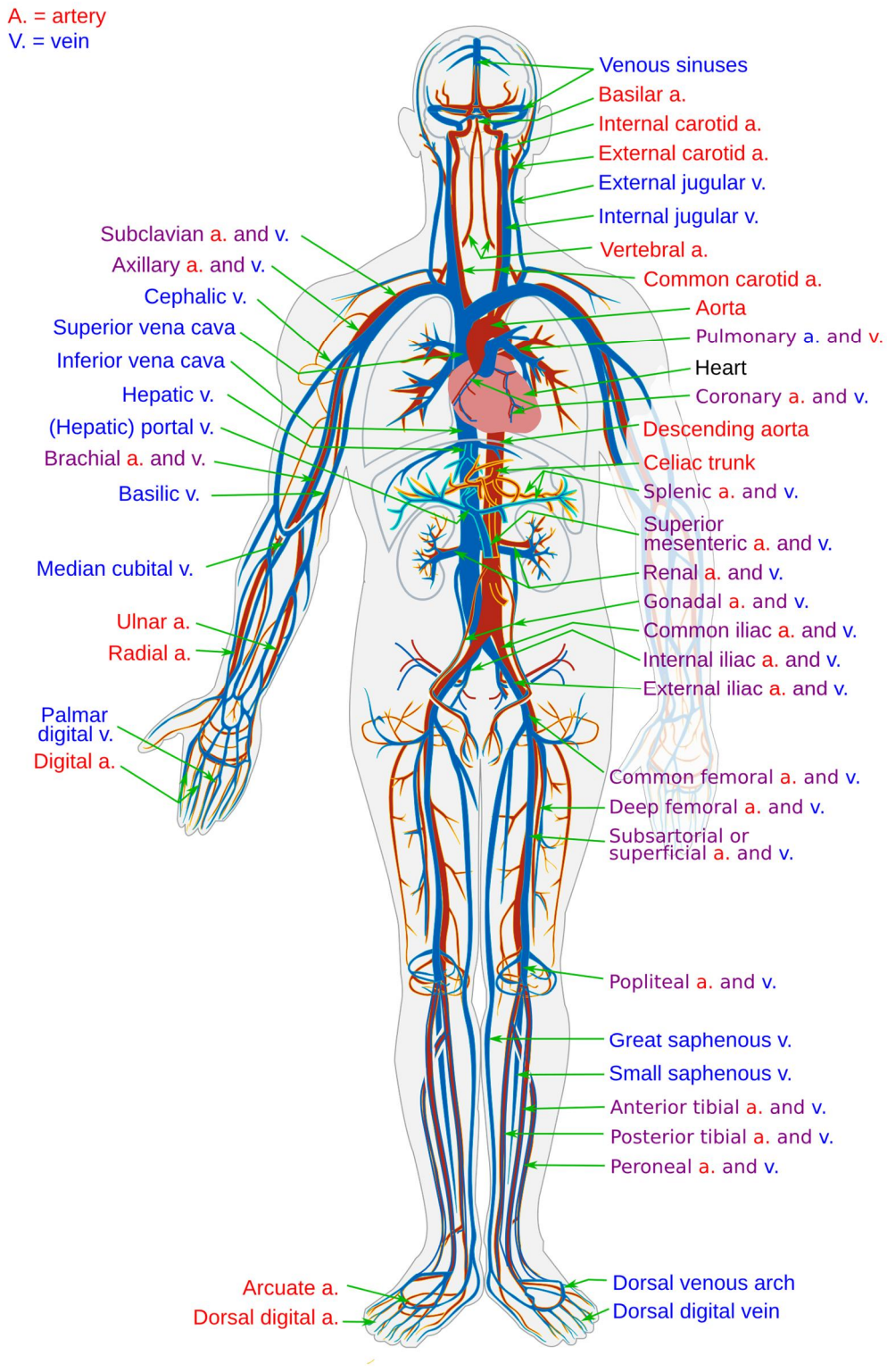

Figure 1: The conceptual scheme of human vascular system [9].

1.2 Vascularization demand and current strategies

The need for organ transplants is rapidly increasing. In 2021, there are 106,810 active patients on the waiting list for a solid organ transplant in the United States [10]. The gap between the number of patients waiting for organ transplantation and the number of donated organs available has considerably expanded in recent years, resulting in countless patient fatalities and increasing socioeconomic costs [11]. Biofabrication strategies that combine biocompatible materials, chemicals, and living cells have recently made noticeable development to solve this problem [12]. However, the necessity for vascularization is the most common challenge to clinical translation of three-dimensional (3D) tissue-engineered structures. In order to sufficiently get oxygen, nutrients, and get rid of metabolic waste, living cells need to be within 200 micrometers of a blood supply [13]. This ensures long-term survival and functionality [13, 14]. Hence, adequate integration of vasculature in 3D tissue-engineered constructs is the requisite objective to prevent hypoxia and cellular necrosis.

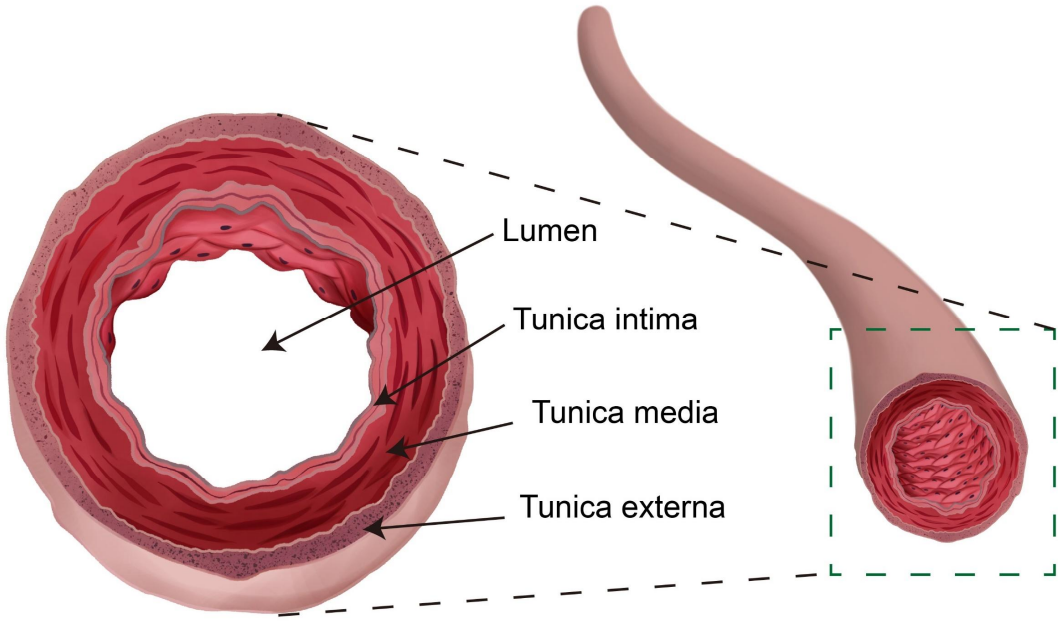

Figure 2: General structure of blood vessels.

Many attempts to integrate vascular networks inside 3D artificial tissue constructions have been studied. One among them is the 3D bioprinting technique. Biomaterials, cell sources, and angiogenic growth factors have been used to form vasculature using 3D bioprinters. This strategy may be classified as direct or indirect printing [15].

In the indirect strategy, to construct 3D vascular-like perfusable channels, fugitive hydrogels such as carbohydrate glass [16], gelatine [17], agarose [18], or Pluronic F127 [19] are printed and subsequently dissolved using chemical or heat stimulation. Once dissolved, ECs are gently spread entire the lumen channels for endothelialization. However, the dissolving process can affect to the proliferation and differentiation of the ECs [20-22].

In the direct strategy, specialized microfluidic nozzles are used to directly print microtubular cell-laden scaffold [15, 23]. The vascular cells may be seeded inside the printed structure, unlike the indirect strategy. The direct technique, which uses specialized microfluidic nozzles, may generate smaller scaffolds than the indirect method. This advantage could improve the 3D bioprinting resolution [24]. In 2018, Pi *et al.* published a technique for cannular tissue fabrication, such as micro-blood vessels and urothelial tissues, using a direct multilayer bioprinting approach [25]. To increase cellular proliferation and migration, they utilized a customized bioink comprised of alginate, gelatine methacryloyl (GelMA), and an eight-arm poly(ethylene glycol) acrylate with a tripentaerythritol core (PEGOA). However, UV illumination was used to polymerise GelMA and PEGOA, which then interacted with mammalian cells in various ways, causing cell death, erythema, and cancer [26-28]. To create channels with an EC monolayer, Gao *et al.* proposed a tissue-specific alginate-based bioink and a 3D coaxial cell printing approach [29, 30]. By employing an ionic crosslinking approach, that group was able to avoid the constraints of UV photopolymerization. However, to re-establish native blood vessels, an EC monoculture is inadequate [6, 31]. More

importantly, the hydrogels used in those current studies are not natural ECMs, they are inadequate to supply the best microenvironment for cell-cell connection and 3D cellular interactions. In consequence, those cells in such synthetic scaffolds have hardly demonstrated inherent morphologies and biological functions, which led to low mechanical properties [32, 33]. Recently, natural biomaterials such as type I collagen [33], and decellularized ECM (DECM) [25, 30] have been used to address these limitations due to their high porosity and specific peptide sequences. These materials possess specific peptide sequences that can be recognized by cells' surface receptors as a substrate for cell adhesion and migration. Especially, type-I collagen has been widely used as a powerful coating material for cell-culture applications [34, 35]. Furthermore, the stiffness of type-I collagen is higher compared with that of fibrin and Matrigel at the same concentration [36, 37].

1.3 Objectives

In this dissertation, the co-culture of human vascular smooth muscle cells and human endothelial cells was applied with the coaxial laminar flow extrusion technique to continuously print long human vascular tissues at the micro scale (< 1 mm diameter). Micro blood vessel-like structures were generated from collagen-based bioinks using a coaxial microfluidic nozzle without ultraviolet radiation. Human umbilical vein endothelial cells (HUVECs) and human aortic smooth muscle cells (HASMCs) were co-seeded within such tubular scaffolds to functionalize the structures. The printability, perfusability, and functional properties including angiogenesis, ECM secretion of the vessel were investigated.

1.4 Dissertation organization

The dissertation's structure will be divided into 3 chapters as below:

Chapter 1 focuses on the literature overview including the general of the human vascular system, microscopic vascular tissues. Next, a review about

vascularization demand, current strategies and, their limitations. The final parts describe the objectives and dissertation organization.

Chapter 2 describes the coaxial printing of double-layered and free-standing blood vessel analogues without ultraviolet illumination for high-volume vascularised tissue.

Chapter 3 summarizes obtained achievements, limitations in this dissertation and gives out some feasible solutions and perspectives.

Chapter 2:
Coaxial printing of double-layered and free-standing blood vessel analogues without ultraviolet illumination for high-volume vascularised tissue

2.1 Background

In the direct strategy, to reconstruct microchannels with an EC monolayer, Gao *et al.* developed a tissue-specific alginate-based biomaterial and a 3D coaxial cell extrusion method [29, 30]. Using the ionic crosslinking approach, their technique avoided the constraints of UV photopolymerization. However, an EC monoculture alone is inadequate to reconstitute native blood vessels.

On a specialized *in vitro* co-culture plate, Liu *et al.* showed the impact of ECs on the morphology change, proliferation, and differentiation of SMCs [38]. However, the importance of co-culture in the field of 3D bioprinting remains not thoroughly understood. To reconstruct natural microscopic venous or arterial architecture, ECs and SMCs must be co-cultured on a tubular scaffold. By modulating vasoactivity through cellular relaxation and contraction [39], the co-culture of ECs and SMCs plays an important role in vascular maintenance, development, and remodelling [40]. To compensate for degraded ECM, ECs and SMCs jointly produce new ECM [41] and angiogenic growth factors to stimulate tubulogenesis and vasculogenesis. Meanwhile, The luminal surface of the scaffold is covered with a monolayer of ECs. Both ECs and SMCs collaborate to create vasoactive molecules including platelet-derived growth factor (PDGF) and endothelin, which help SMCs proliferate, differentiate, migrate, and newly secrete ECM. [41-45].

In this chapter, we used a coaxial microfluid nozzle to print a coaxially layered blood-vessel-like scaffold comprising human umbilical vein endothelial cells (HUVECs) and human aortic smooth muscle cells (HASMCs) without UV illumination (Figure 3). The nozzle was created to extrude the coaxial scaffolds in a smooth and controlled manner at the microscale. To illustrate the benefits of our co-culture approach for ECM synthesis, cell differentiation, and angiogenic factor secretion, the transcriptional expressions of genes for collagens I, III, and IV, smoothelin, alpha-actin, and vascular endothelial growth factor (VEGF) were

examined. The scaffolds' perfusability was observed using a special connector. The scaffolds' mechanical characteristics, such as toughness and deformation response, were also assessed. The proposed method might be used to print a vascularized organ.

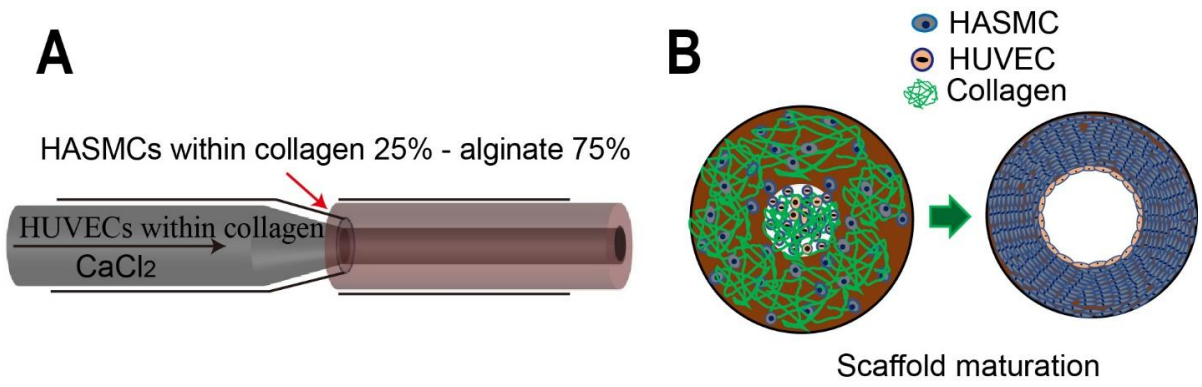

Figure 3: A schematic of the proposed method. Suspended HUVECs and type I collagen (3 mg/mL) containing $CaCl_2$ (100 mM) were introduced as the core, and a mixture of HASMCs and a collagen-alginate hydrogel (25:75) was pumped as the shell layer.

2.2 Materials

In this chapter, we obtained calcium chloride anhydrous (CaCl2, 2507-1400, DEAJUNG, Republic of Korea), sodium alginate (13035S1201, JUNSEI, Japan), native type I collagen (IAC-50, KOKEN, Japan), silicone elastomer base, silicone elastomer curing agent (Sylgard, 184 silicone elastomer kit, Dow Corning Corporation, U.S.A.), food-dye (WILTON, Republic of Korea), red fluorescence beads (S-FluoRed-Fi198, microParticlesGmbH, Germany), green fluorescence beads (PS-FluoGreen-Fi199, microParticlesGmbH, Germany), blue fluorescence beads (S-FluoBlue-Fi165, microParticlesGmbH, Germany), HASMCs (PCS-100-012, cryopreserved, ATCC, U.S.A.), HUVECs (PCS-100-010, cryopreserved, ATCC, U.S.A.), vascular smooth muscle cell growth kit (PCS-100-042, ATCC, U.S.A.), vascular cell basal medium (PCS-100-030, ATCC, U.S.A.), endothelial cell growth kit-VEGF (PCS-100-041, ATCC, U.S.A.), high

glucose DMEM (11995073, Thermo Scientific, U.S.A.), LIVE/DEAD™ viability/cytotoxicity kit for mammalian cells (L3224, Thermo Scientific, U.S.A.), ZO-1 monoclonal antibody (ZO1-1A12, 33-9100, Thermo Scientific, U.S.A.), goat anti-mouse IgG (H+L) highly cross-adsorbed secondary antibody — Alexa Fluor plus 488 (A32723, Thermo Scientific, U.S.A.), cluster of differentiation 31 (CD31) monoclonal antibody (MA5-13188, Thermo Scientific, U.S.A.), cytoplasmic probes — CellTracker™ red CMTPX (10 μM, C34552, Thermo Scientific, U.S.A.) and CellTracker™ green BODIPY™ dye (10 μM, C2102, Thermo Scientific, U.S.A.), 4′,6-diamidino-2-phenylindole (DAPI, NucBlue® Live ReadyProbes™ Reagent, Thermo Scientific, U.S.A.), paraformaldehyde (P6148, Sigma-Aldrich, U.S.A.), blocker bovine serum albumin (BSA) (37525, Thermo Scientific, U.S.A.), Triton-X100 (T8787, Sigma-Aldrich, U.S.A.), and gene-specific primers (Table 1, Bioneer, Republic of Korea).

Table 1: Gene-specific primers.

Gene name	Forward primer sequence (5′-3′)	References
Collagen I	F: ATGTGGCCATCCAGCTGAC R: TCTTGCAGTGGTAGGTGATGTTCT	[38, 46]
Collagen III	F: CCCAGAACATCACATATCAC R: CAAGAGGAACACATATGGAG	[47]
Collagen IV	F: TGGTGACAAAGGACAAGCAG R: TAAGCCGTCAACACCTTTGG	[48, 49]
Smoothelin	F: CCCTGGCATCCAAGCGTTT R: CTCCACATCGTTCATGGACTC	[38]
Alpha-actin	F: CATCACCAACTGGGACGA	[38]

	R: GGTGGGATGCTCTTCAGG	
VEGF	F: GCACCCATGGCAGAAGGAGG R: CCTTGGTGAGGTTTGATCCGCATA	[43]
Beta-actin	F: TCCCCCAACTTGAGATGTATGAAG R: TCCCCCAACTTGAGATGTATGAAG	[48]

2.3 Methods and results

2.3.1 Hydrogel

One of the primary components of ECM is type I collagen [50]. type I collagen matrix allows cells to proliferate, migrate, and differentiate more effectively than alginate [33]. However, alginate's gelation time is much more quickly than that of collagen. Herein, to create coaxial two-layered scaffolds, several collagen and alginate combinations were tested.

Sterile sodium alginate solution was prepared using a technique described by Ning et al. [51]. Briefly, a 0.6% weight/volume (w/v) solution was prepared by dissolving sodium alginate powder in deionised water then carefully filtered using a 0.22 μm bottle-top filter (J1.F204.500, SCI-lab, Republic of Korea) under an uncontaminated condition. The filtered solution was frozen overnight at 80 degrees Celsius (°C) and then lyophilised for at least 72 hours under a sterile condition. The dried alginate was redissolved in phosphate-buffered saline (PBS) at 1.8% (w/v) without calcium chloride ($CaCl_2$) and magnesium chloride ($MgCl_2$) then supplemented with 145 mM sodium chloride (NaCl).

We followed a video protocol published by AIM Biotech (Singapore) to prepare the type I collagen solution [52]. Briefly, Type I collagen (5 mg/mL) was supplemented with 10% 10X PBS and neutralized with 0.5 N sodium hydroxide

(NaOH). To create a 3 mg/mL type I collagen solution, deionized water was added to the solution. All procedures were performed at 2-10 °C to prevent the gelation of the collagen.

At varied volume ratios, type I collagen (3 mg/mL) and sodium alginate (1.8% w/v) were blended (100:0, 80:20, 25:75, 20:80, and 0:100). Scanning electron microscopy (SEM) was used to examine the microstructures of the alginate and collagen matrices. Firstly, the blended materials (1 mL) were pipetted into a 2-mL tube then 500 µl of 100 mM $CaCl_2$ were added and incubated at 37 °C for 12 hours at least. The residual $CaCl_2$ was removed entirely after gelation, and the gelated hydrogel was rinsed twice with PBS. The hydrogels were then immersed in liquid nitrogen for 3 minutes for the snap freezing process before being lyophilised. An Emitech K575X sputter coater was used to metal coat the dessiccate hydrogels (Quorum Technologies Ltd., United Kingdom). Micromagnifications were obtained using a SU8220 Cold FE-SEM (Hitachi High Technologies Korea Co., Ltd., Republic of Korea).

SEM magnifications of the blended collagen and alginate hydrogels are shown in Figure 4a. The fibrous structures indicated collagen matrices while alginate appeared in monolithic lumps. The hydrogels containing 80% and 100% collagen had a more linked network than the others.

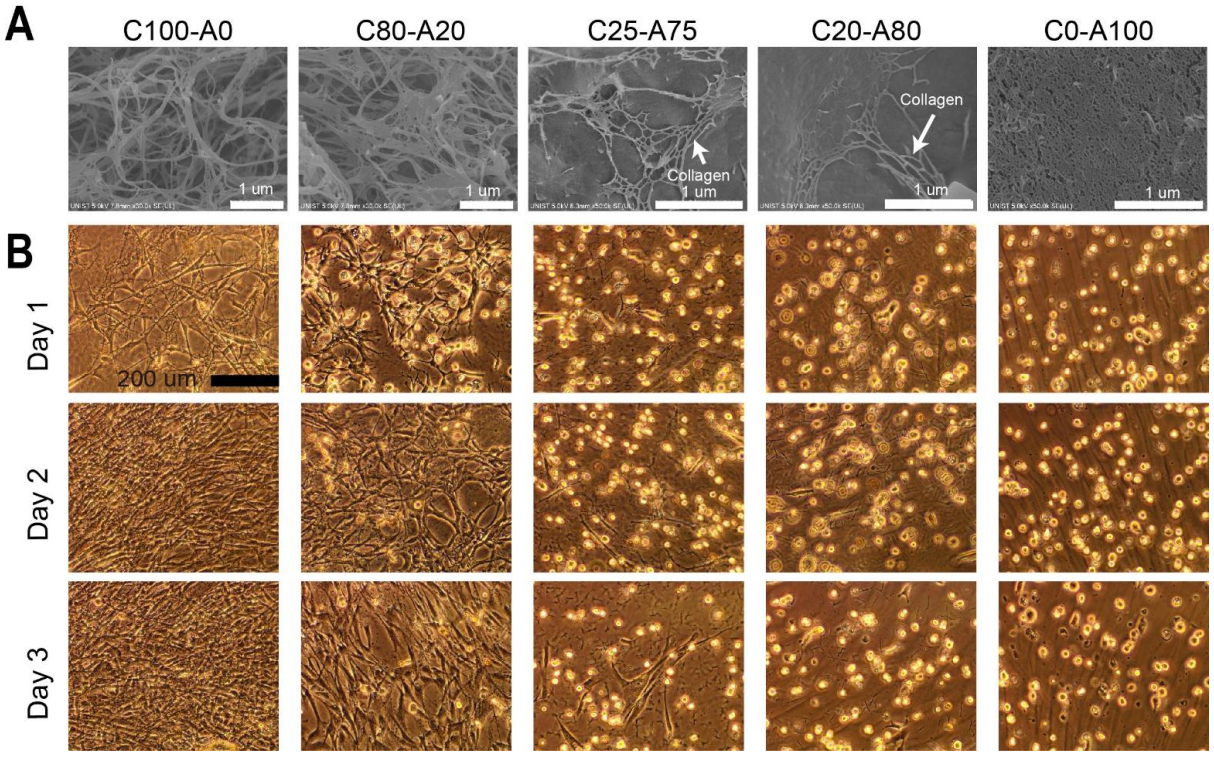

Figure 4: The collagen-alginate hydrogel. (a) The microstructures of the collagen-alginate blends (scale bar: 1 μm). (b) HASMCs inside the collagen-alginate scaffolds (scale bar: 200 μm).

Inside the collagen and alginate hydrogels, HASMCs were laden and then they proliferated. Their morphology and viability were observed and investigated to see whether they might be used as tunica intermedia. Frozen HASMCs were thawed and expanded in vascular cell basal medium supplemented with a vascular smooth muscle cell growth kit at 37 °C, 5% CO_2. The cells were passaged with a 0.05% trypsin ethylenediaminetetraacetic acid (EDTA) before they reached 80% confluence. The HASMCs were harvested and suspended in the collagen–alginate blends at a density of about 2×10^6 cells/mL after they achieved around 80% confluence within 6 to 12 passages. To make a 3D scaffold, 800 μL of the cell suspension was pipetted uniformly onto a 35-mm cell culture dish and then gelled with 100 mM $CaCl_2$. The gelated cell-laden hydrogels in the 35-mm dish were roughly 850 μm thick. The scaffolds were rinsed three times with PBS after the gelation. Following that, 1.5 mL of pre-warmed fresh HASMC media was

added to the cell-laden scaffold, which was subsequently incubated at 37 °C with 5% CO_2.

An IX53 inverted microscope (Olympus, Japan) was used to observe the cell growing. Figure 4b shows images of the HASMCs' morphology within the blended collagen and alginate hydrogels. Higher collagen ratios resulted in more elongated cells. The HASMCs unfurled their shape considerably more quickly in hydrogels containing 80% and 100% collagen than with those containing lower collagen ratios.

To show cell viability, the cell-laden scaffold was stained in PBS with 0.2% ethidium homodimer-1 (2 mM) in dimethyl sulfoxide (DMSO)/H_2O at 1/4 (v/v) and 0.05% calcein-AM (4 mM) in anhydrous DMSO. The samples then were were treated with DAPI for 30 minutes at 37 °C and 5% CO_2 for nucleus staining. The cell-laden scaffold was then rinsed five times in PBS before being observed with an Olympus BX53 digital upright microscope (Olympus, Japan) with a 4x objective lens. ImageJ software (Fiji, NIH Image, U.S.A., version 1.51h) was used to analyze ten pictures (5 per experiment). The fluorescent signal of the stained cells was divided into a red channel (dead cell signal) and a green channel (living cell signal) for the cell viability calculation, and the intensity of the two channels was evaluated using ImageJ. Using the ratio of green intensity to total intensity, the percent viability was estimated from the observed signal intensity:

$$viability = \frac{green\ intensity}{green\ intensity + red\ intensity} \times 100 \qquad \text{(Equation 1)}$$

In all mixing conditions, more than 83% of the HASMCs inside the hydrogel were alive, with no significant differences (Figure 5). This results indicated that none of the collagen and alginate mixes were harmful to HASMCs.

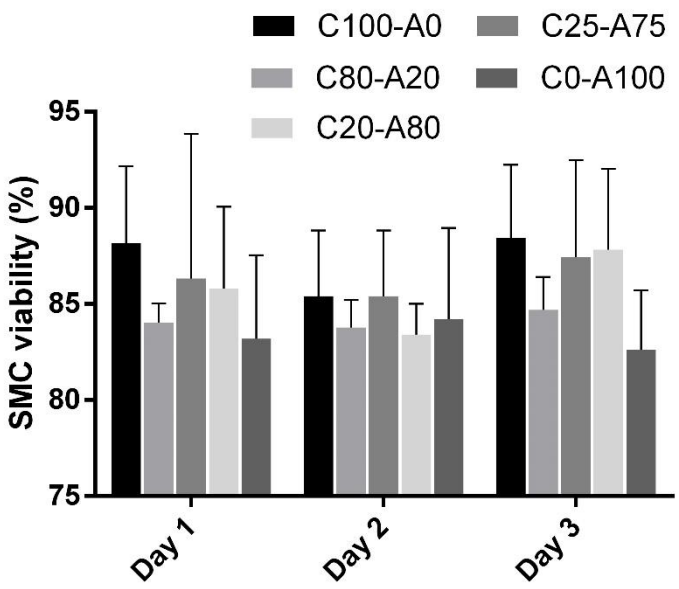

Figure 5: The HASMC viability in 3D flat scaffolds with different collagen rati os over three days (sample size n = 10 from 2 experiments).

2.3.2 Cell-laden core-shell scaffold generation and printing

We developed and fabricated a coaxial laminar microfluid generator, as shown in Figure 6a–c, to create the layered tubular scaffold of HASMCs and HUVECs. The device comprised three micro-glass tubes (580 µm inner diameter (ID), 1B100-6, World Precision Instruments, U.S.A.): one vertical inlet for shell material pumping; one horizontal inlet for core material pumping; and one outlet. A PC-10 puller (NARISHIGE Group, U.S.A.) was used to thermally draw a glass capillary to a 220 µm ID for the horizontal inlet. As illustrated in Figure 6b, the horizontal inlet's tapered tip was partially inserted into the outlet. All three micro-glass tubes were put together in a cuboid-shaped polydimethylsiloxane (PDMS) body.

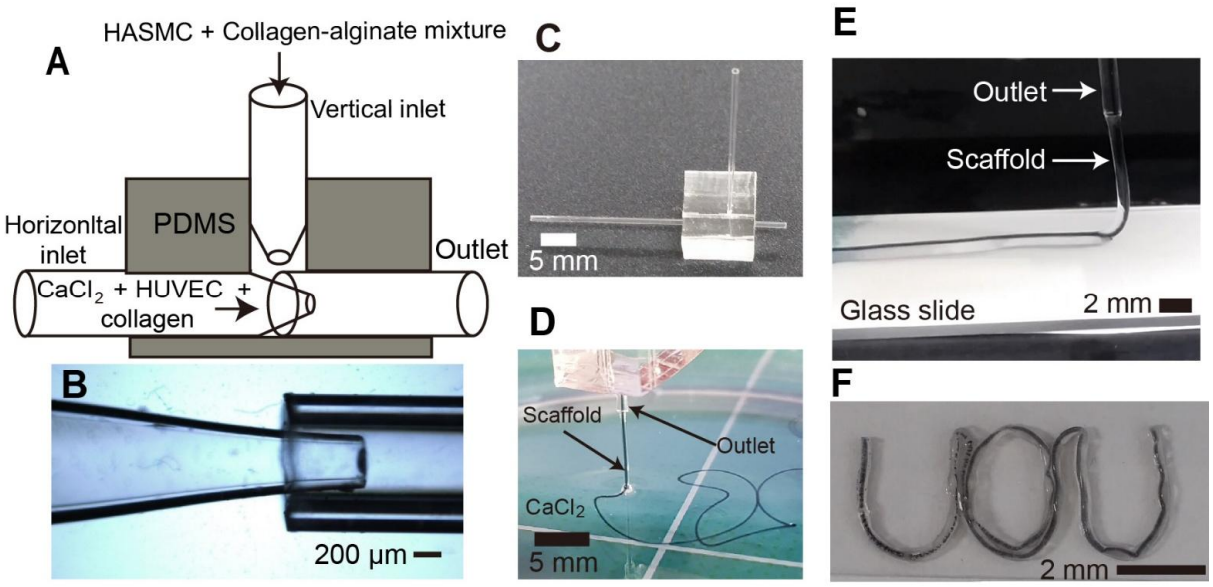

Figure 6: The proposed coaxial microfluid nozzle and experimental configuration. (a) Schematic of the proposed generator, which comprised three glass capillaries: a vertical inlet for pumping the shell-layer materials, a horizontal inlet for pumping the core materials, and an outlet. All three capillaries were assembled in a cuboid-shaped PDMS block. (b) Magnified view of the junction area. (c) The fabricated nozzle. (d) The scaffold formation with a $CaCl_2$ dish. (e) The printability tests. (f) The printed "UoU" pattern.

As illustrated in Figure 6d–e, the proposed printing system was set up to test core-shell scaffold extrusion and printability. It comprised two syringe pumps for the core and shell materials that were connected to a fabricated coaxial laminar microfluid generator. The generator was fixed on a manual x-y stage controller (binocular microscope, ML5000, Meiji Techno, U.S.A.). To prevent the collagen from gelling before printing, two 5 mL syringes (Kovax, Republic of Korea) containing the core and shell materials were placed on ice (0 – 10 °C). The horizontal and vertical inlets were used to introduce the core and shell materials, respectively. As shown in Figure 6d–f, crosslinking interactions between Ca^{2+} ions and sodium alginate chains resulted in the formation of core-shell scaffolds. After alginate gelation, residual $CaCl_2$ was rinsed off the gelated scaffold using

PBS. The scaffold was then incubated for at least 15 minutes at 37°C to allow collagen gelation.

Despite the fact that the laminar microfluid generator was well-designed, the viscosity of the fluid had an impact on the flow pattern. Indeed, the HASMCs were more compatible with a greater collagen ratio in the collagen and alginate blend; however, a high collagen ratio caused the mixture less viscous and prevented it from forming a laminar microflow. When evaluated across five trials, blends with a 30% collagen ratio failed half of the time while blends with a less than 25% collagen ratio succeeded in almost every trial (Figure 7). Because of its cell biocompatibility and ability to generate laminar microflow, a blend with a collagen-alginate ratio of 25:75 was chosen as the shell layer material.

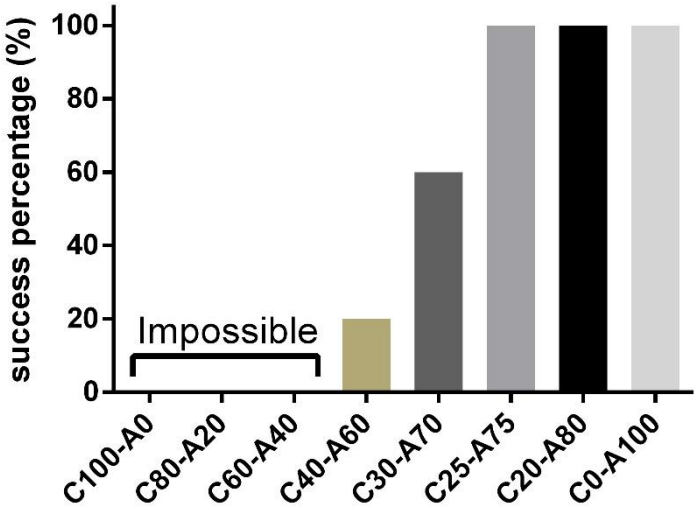

Figure 7: The success rate of tubular scaffold formation with different collagen ratios (trial number n = 5).

The 25:75 blend of collagen and alginate was printed continuously in the layered core-shell structure (Figure 6d–e and Supplementary Movies S1 and S2). Figure 6d and Supplementary Movie S1 show that the core-shell laminar flow was pumped out into a $CaCl_2$ dish as an arbitrary structure. Meanwhile, Figure 6e and Supplementary Movie S2 illustrated a straight scaffold printing, Figure 6f

showed a “UoU” (University of Ulsan) pattern printing on a glass slide. Because of the rough stage and manual control, the patterns have a slight lack of accuracy. Nonetheless, these illustrations show that the suggested technology is capable of 3D bioprinting.

2.3.3 HASMC shell layer scaffold

To examine the cellular interaction between HASMCs and HUVECs, three types of the scaffold were created and assessed: (1) a HASMC shell layer scaffold, (2) a HUVEC core scaffold, and (3) a co-culture scaffold made of a HUVEC core and HASMC shell layer (the HUVEC–HASMC scaffold). The HASMCs were harvested and suspended at about 2×10^6 cells/mL in a 25:75 collagen and alginate mixture. This mixture was introduced through the vertical inlet at a rate of 0.7 mL/min as the shell layer material while 300 mM $CaCl_2$ was injected into the horizontal inlet at a rate of 0.1 mL/min as the core material. The scaffold was extruded into a 100 mM $CaCl_2$ dish and rinsed in PBS after 5 minutes in the $CaCl_2$ dish. After that, it was supplied with fresh media (vascular cell basal medium + 10% fetal bovine serum (FBS) + 1% penicillin/streptomycin) and incubated at 37 °C with 5% CO_2. Due to the $CaCl_2$ in the core and dish, the gelated scaffold formed a tubular shape. The HASMCs in the shell layer were assessed for viability, confluency, and contraction behavior. On days 10 and 20, the fluorescence intensities from the green (living) and red (dead) channels of 5 samples from two experiments were quantified using ImageJ to determine viability. Using Wang's technique [53], the confluence was calculated as the ratio of green areas (living) over the total field of vision (Figure 8).

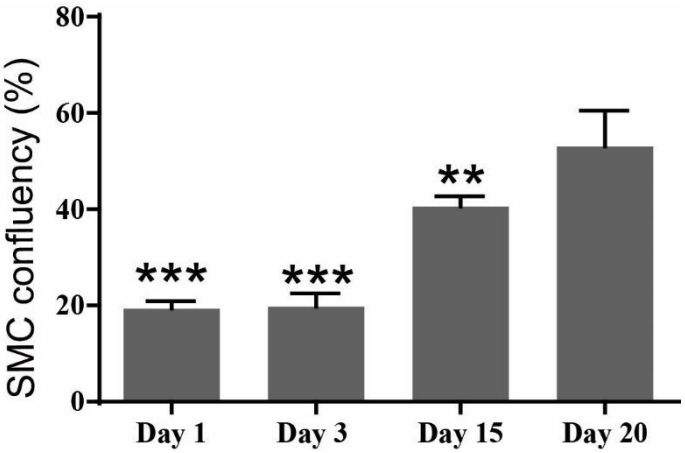

Figure 8: The HASMC confluency in C25-A75 tubular scaffolds over 20 days (** $0.001 < p < 0.01$, *** $p < 0.001$, compared with day 20, sample size $n = 5$ from 2 experiments).

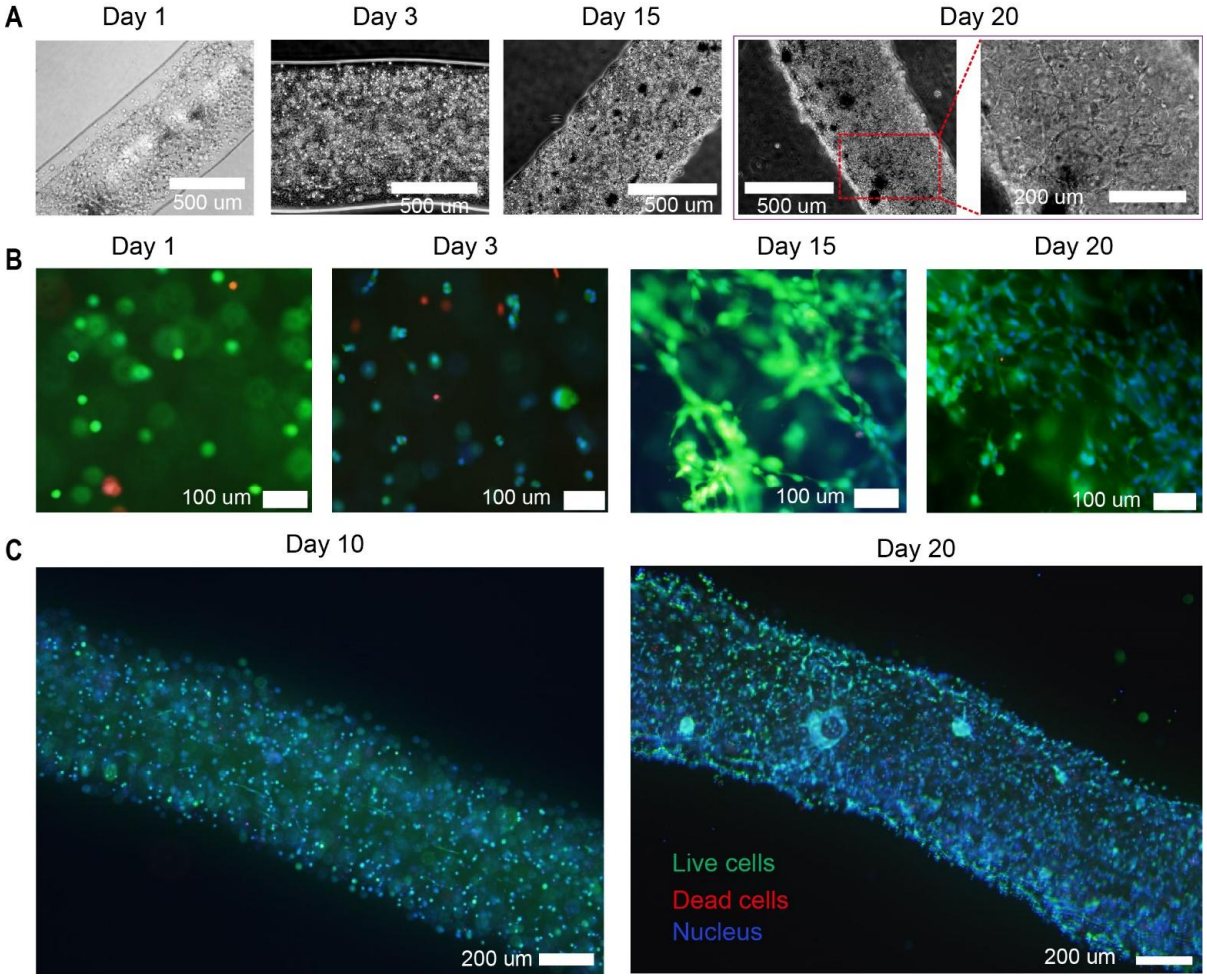

Figure 9: The HASMC shell layer scaffold. (a) Bright-field magnifications of the

HASMC scaffold. (b) 10X live/dead fluorescence magnifications of the HASMC scaffold (green, live cells; red, dead cells; blue, nuclei). (c) 4X live/dead fluorescence images of the HASMC scaffold on day 10 and day 20**.**

Figures 9a and 9c demonstrate the morphological changes of HASMCs in the HASMC scaffold over time. The HASMCs existed in spherical shapes until day 3 (Figure 9b). They became longer and stuck together over 15 days. The viability of HASMCs was above 90% on day 10, with no significant change on day 20 (p = 0.849, Figure 10).

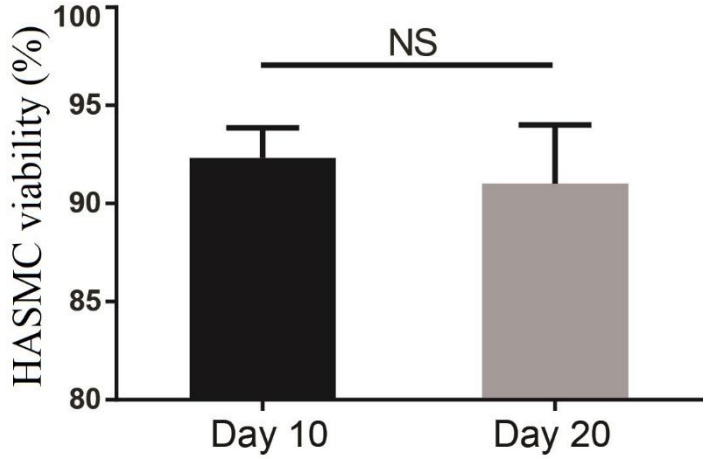

Figure 10: The HASMC viability in tubular scaffolds with different collagen ratios on days 10 and 20 (NS: no significance, sample size n = 5 from 2 experiments).

2.3.4 HUVEC core scaffold

Frozen HUVECs were thawed and expanded at 37 °C in a cell incubator containing 5% CO_2. The HUVECs were grown in vascular cell basal media supplemented with an endothelial cell growth kit-VEGF throughout the expansion. The HUVECs were collected and dispersed at low and high densities of approximately 3.5×10^6 and 1.7×10^7 cells/mL in 3 mg/mL type I collagen. At a rate of 0.1 mL/min, both suspensions were introduced into the horizontal inlet as the core material. Meanwhile, the shell material was a mixture of 25%

collagen and 75% alginate pumped at a rate of 0.7 mL/min through the vertical inlet. Once gelled, the HUVEC core scaffold was washed in PBS and supplied with fresh media and incubated at 37 °C, 5% CO_2.

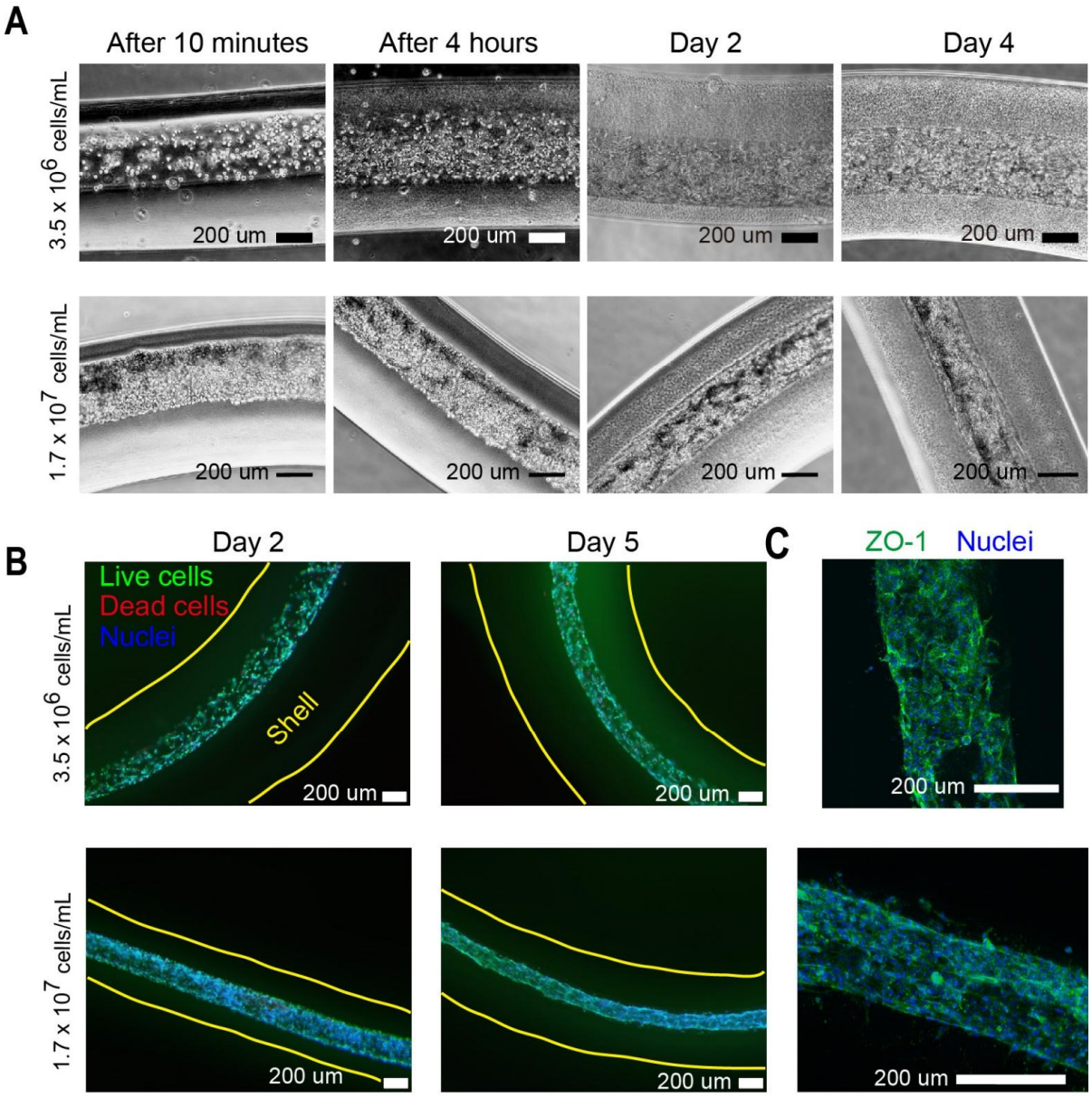

Figure 11: The HUVEC core scaffold. (a) Bright-field magnifications of HUVEC confluence at two different cell densities. (b) Live/dead fluorescence images of the HUVEC confluence at two different cell densities. (c) Confocal immunostained image of ZO1 signals.

Figure 11a shows bright-field observations of the HUVEC core inside the gelated scaffold. The seeded HUVECs seemed to be non-uniformly settled for up to 4 hours after formation. We hypothesized that the seeded HUVECs shrunk due to the collagen's poor gelation rate. However, two days later, the HUVEC core seemed to have a higher cell density inside the live/dead fluorescence pictures, which was more densely or evenly packed (Figure 11b). More than 88% alive cells in the high-density HUVEC core, as well as more than 85% alive cells in the low-density HUVEC core (Figure 12).

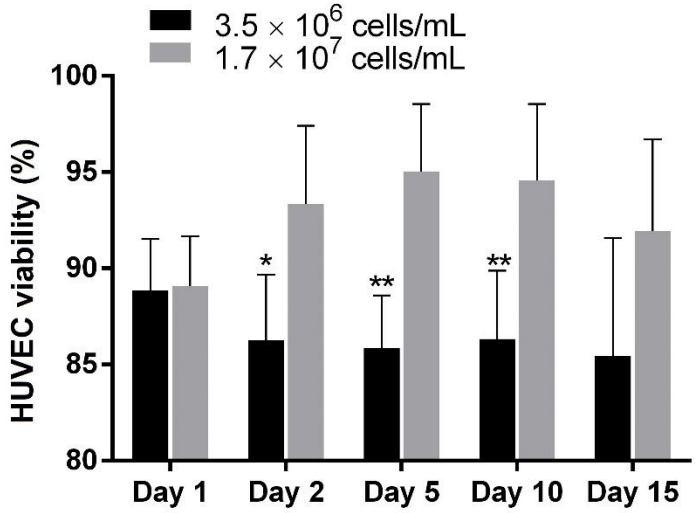

Figure 12: HUVEC viability in C25-A75 tubular scaffolds with two HUVEC densities over 15 days (* $0.01 < p < 0.05$, ** $p < 0.01$, between the low and high cell densities, n = 10 from 2 experiments).

Tight junctions were checked using ZO-1 immunofluorescence labeling. The HUVEC core scaffold was fixed for 30 minutes with 4% paraformaldehyde (P6148 Sigma-Aldrich, USA), permeabilized for 5 minutes with 0.5% Triton-X100, and blocked for 15 minutes at room temperature (RT) with 3% BSA. The scaffold was then treated with ZO1-1A12 monoclonal antibody overnight at 4 °C. The scaffold was then incubated for 90 minutes at RT with a goat anti-mouse IgG (H+L) highly cross-adsorbed secondary antibody, Alexa Fluor plus 488, at a dilution of 1:1000. For 10 minutes, the nuclei were counterstained with DAPI.

The primary and secondary antibody concentrations were chosen according to the manufacturer's recommendations. The stained scaffold's ZO-1 signals reveal tight junctions within the HUVEC core, as seen in Figure 11c.

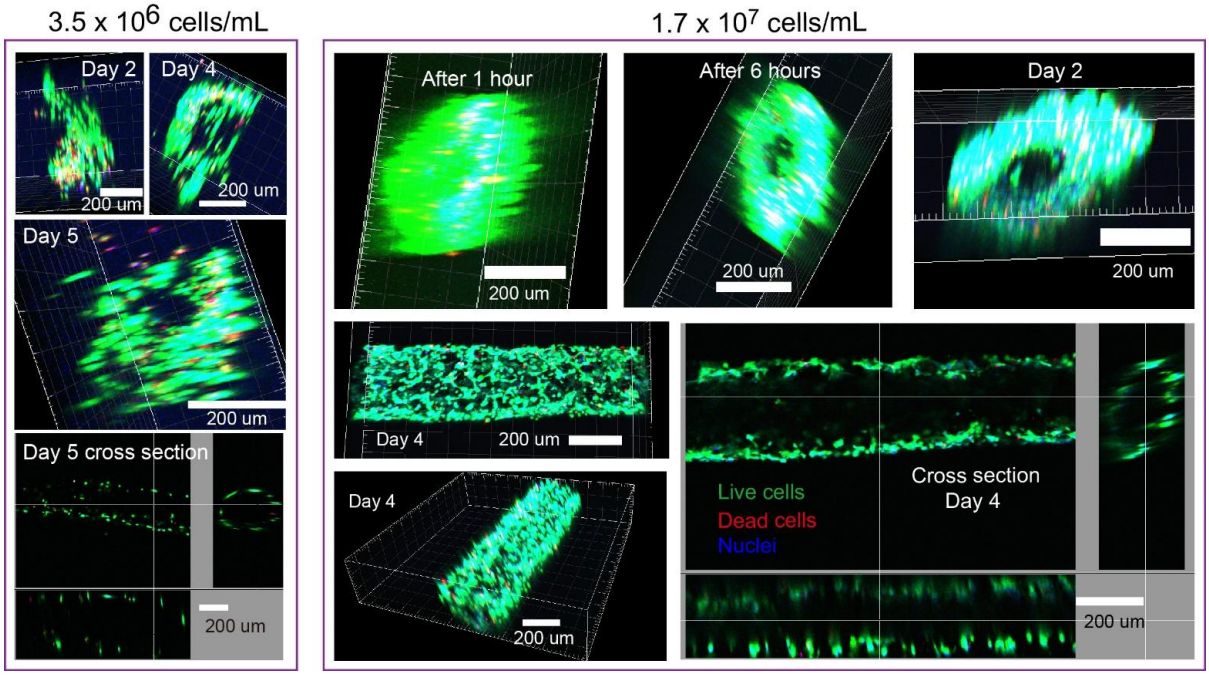

Figure 13: The monolayer formation of the HUVEC core at two different cell densities. The lumen structure was observed in the high-density HUVEC core six hours after generation, and it became more visible on days 2 and 4, whereas it took longer than two days for the low-density core to form a hollow channel.

Confocal observations of the live/dead-stained HUVEC core scaffold are shown in Figure 13 and Supplementary Movie S3. Six hours after creation, a hollow channel was observed in the high-density HUVEC core. On days 4 and 5, cross-sectional images of the high- and low-density HUVEC cores indicate a cell monolayer and a secure channel structure.

2.3.5 HUVEC core and HASMC shell layer (HUVEC–HASMC) scaffold

The core material was a combination of about 1.7×10^7 HUVECs/mL and 3 mg/mL type I collagen. Meanwhile, the shell material was given as a mixture of about 2×10^6 HASMCs/mL and a 25:75 collagen/alginate blend. The core and

shell materials had flow rates of 0.1 mL/min and 0.7 mL/min, respectively. After extrusion, the extruded scaffold was rinsed with PBS, supplied fresh media, and incubated at 37 °C, 5% CO_2. To observe the stratification of the HUVECs and HASMCs, before creating the HUVEC–HASMC scaffold, the HASMCs and HUVECs were washed once with PBS, centrifuged, and incubated with a cytoplasmic probe and 10 M CellTrackerTM Red CMTPX and CellTrackerTM Green BODIPYTM dyes for 35 minutes according to the manufacturer's instructions.

The HUVEC–HASMC scaffold was photographed over time in Figure 14. The HUVCEC core and HASMC shell layer were not visible under a bright field immediately after creation (Figure 14a), but their stratification became much more visible after five hours. The coaxially layered and visually distinct structures may be seen in the fluorescent pictures obtained on day 2 (Figure 14b) and bright-field images taken on day 15 (Figure 14a). The 3D structure of the HUVEC–HASMC scaffold was reconstructed from the images acquired using confocal microscopy, as shown in Figure 14c. At various view angles, a HUVEC lumen of roughly 230 μm in diameter was identified. Due to its approximate thickness of 890 μm, only half of the HASMC shell was observed and rendered.

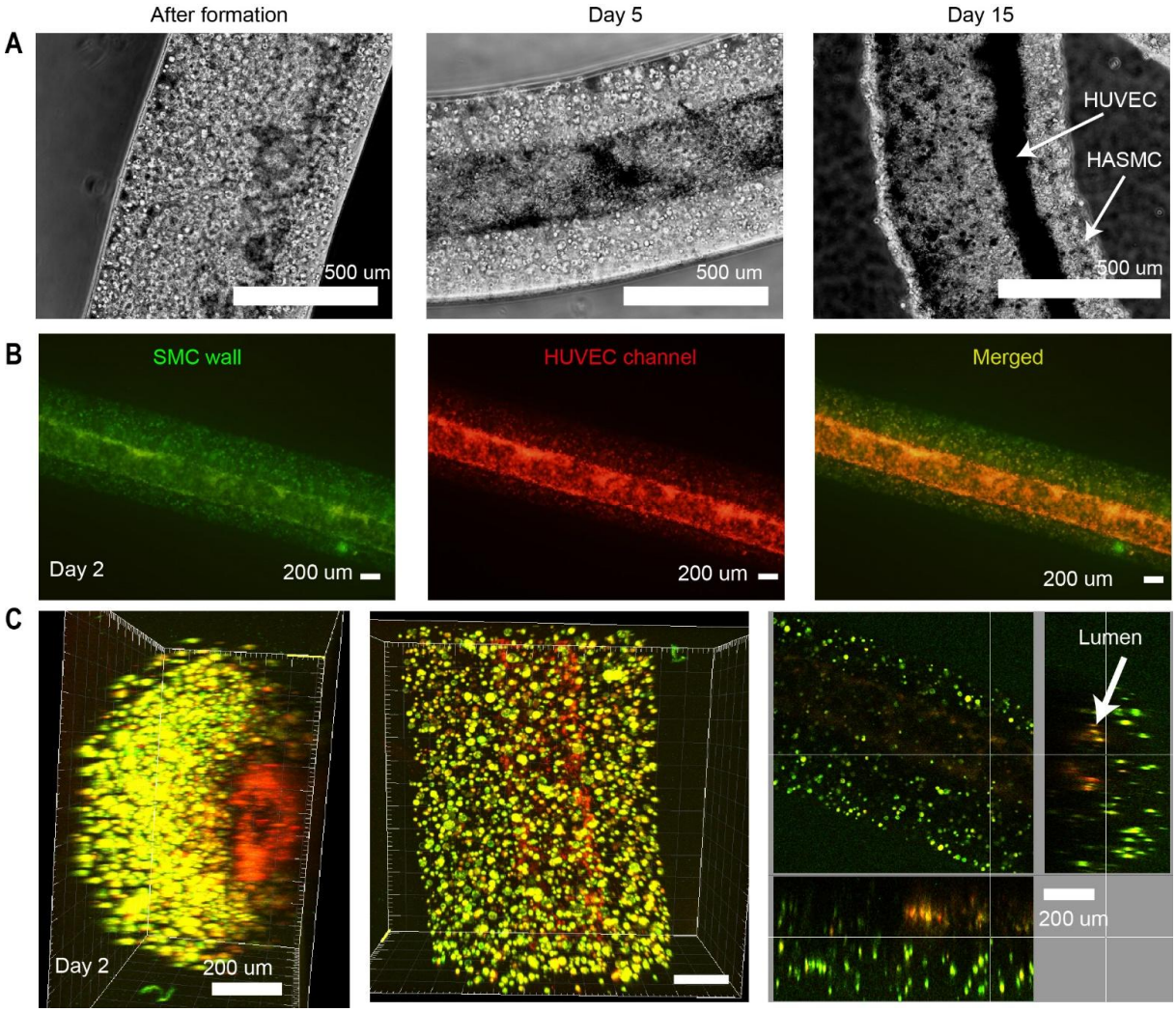

Figure 14: The HUVEC–HASMC scaffold. (a) Bright-field magnification of the co-culture scaffolds for up to 15 days. (b) Fluorescence images of the HUVEC–HASMC scaffold with the cell trackers on day 2. (c) Confocal images of the co-cultured scaffold with the cell trackers on day 2. The HASMC shell layer (yellow) surrounds the HUVEC core (red) with a clear lumen.

2.3.6 Perfusability

An in-house micro-connector was used to pump blue fluorescent beads solution (1:200 in deionised water)into to the tubular scaffolds. As illustrated in Figure 15, the connector comprised three major components: (1) a big glass tube, (2) a mid-sized glass tube, and (3) a small glass capillary. The big glass tube was made of a capillilary (1.15 mm ID and 1.55 mm outer diameter (OD)) (2940210,

MARIENFELD, Germany). It was constricted to an ID of 0.3 mm using a PC-10 puller (Narishige International, U.S.A.). This step allowed to mount the scaffold by connecting the mid-sized glass tube and the small glass capillary together. The ID was 0.58 mm and the OD was 1.0 mm on the mid-sized glass tube (1B100-6, World Precision Instruments, USA). It was narrowed at one end and constricted in the center to accommodate the small glass capillary with an ID of 97.4 μm and an OD of 164.4 μm (1068150020, Polymicro Technologies, Republic of Korea). As illustrated in Figure 15b, two big tapered glass tubes were immobilized and attached as the inlet and outlet at the wall of the cell culture plate (35 mm diameter). The tubular scaffold was sucked into the big tapered glass tube for connection to a pumping system. The scaffold's elasticity allowed for a snug fit within the big tapered glass tube. The tubular scaffold's free end was sucked and secured into the big glass outler tube. The small glass capillary was gently put into the tubular scaffold through the mid-sized glass tube, which was carefully inserted such that the tiny glass capillary was centrally placed inside the tubular scaffold without causing any damage (Figure 15a and 15d). A plastic tube linked a syringe pump with the mid-sized glass tube. Once connected to the pumping system, the connected scaffold was buried in 1.5 mL of 3 mg/mL type I collagen hydrogel (Figure 15c). This step immobilized the scaffold and protected it from structural damage during pumping. On day 3, Figure 15f, 15g, and Supplementary Movie S4 show a constant flow of 0.05 mL/min of the blue beads inside the HUVEC core scaffold and the HUVEC–HASMC scaffold without any leakage.

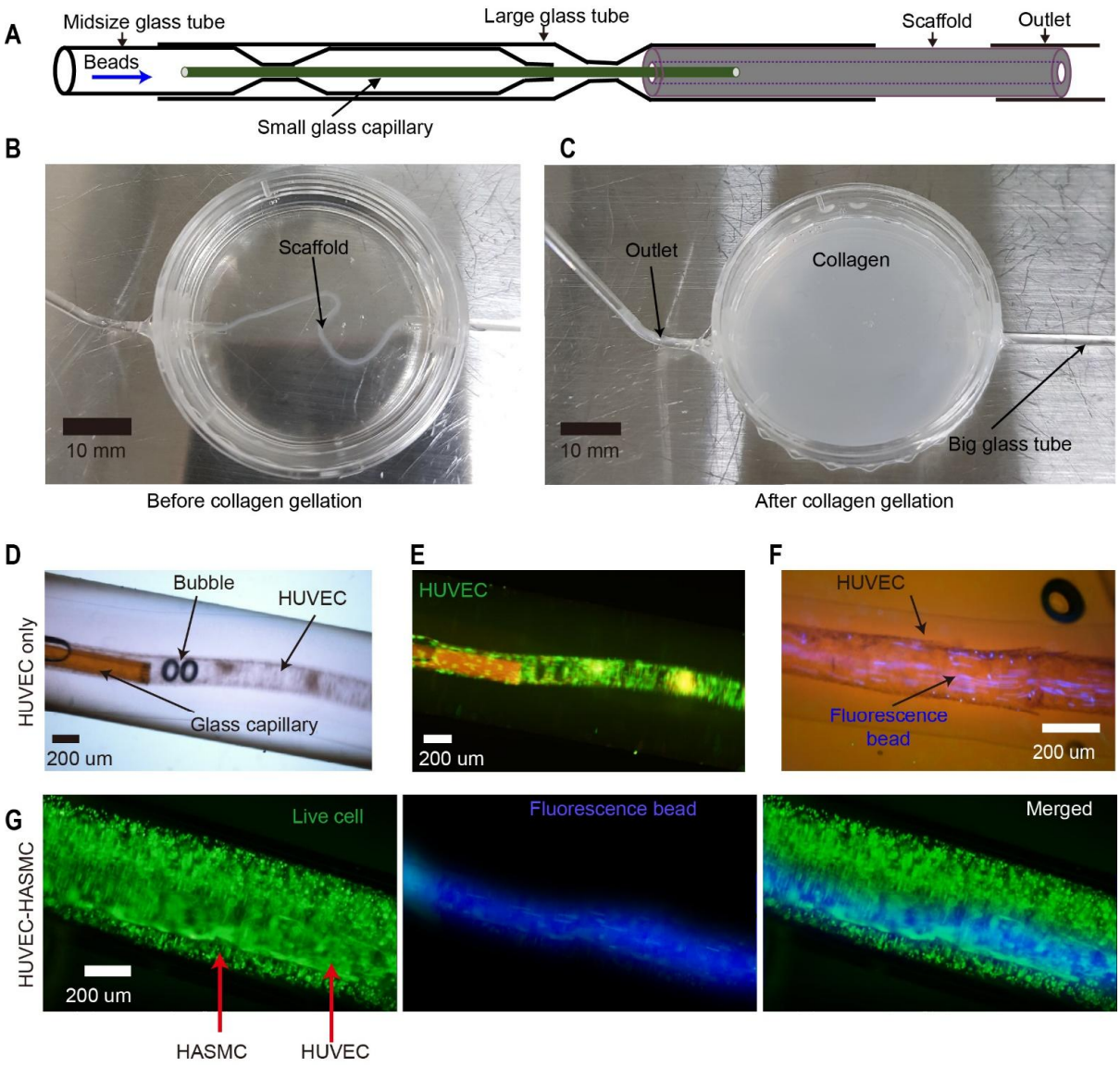

Figure 15: The perfusability test. (a) The proposed connector for the perfusability test. The connector comprised a large glass tube, a mid-sized glass tube, and a small glass capillary. (b–c) The cell scaffold was sucked into the channels of the pumping device, and then 1.5 mL of 3 mg/mL type I collagen was used to bury the scaffold. (d) Bright-field magnifications of the HUVEC scaffold during pumping. (e–f) Fluorescence magnifications of the HUVEC scaffold during pumping. (g) Fluorescence magnifications of the HUVEC–HASMC scaffold during pumping.

2.3.7 Statistical analysis

The mean ± standard deviation is presented as quantified results. The two-tailed student's t-test in Prism 6.01 was used to make comparisons between two groups (GraphPad, U.S.A.). A value of $p < 0.05$ was considered statistically significant. Sample sizes are given in the figure captions.

2.3.8 Mechanical properties

The pumping flow rate was steadily raised in the perfusion test setup (Figure 15) until leakage occurred to assess shear stress endurance. Equation 2 was used to calculate the shear stress as follows:

$$\tau = \frac{32 \times Q}{\pi \times D^3} \times \mu \qquad \text{(Equation 2)}$$

where Q, D, μ were the flow rate, the inner diameter of the scaffold, and the viscosity of water at 20 °C (μ = 1 cP), respectively. Figure 16d–e depicts the changes in ID and OD after 20 days. The shear breaking stress of the HUVEC–HASMC scaffold and the HUVEC scaffold with respect to culture time is shown in Figure 16a. Over the time of 20 days, the shear breaking stress of the HUVEC–HASMC scaffold gradually rose to around 103 dyne/cm^2. The shear breaking stress on the HUVEC scaffold increased similarly until day 15, after which it dropped and by day 20 had achieved a value of around 50 dyne/cm^2. The HUVEC–HASMC scaffold was therefore twice as tough as the HUVEC only scaffold on day 20.

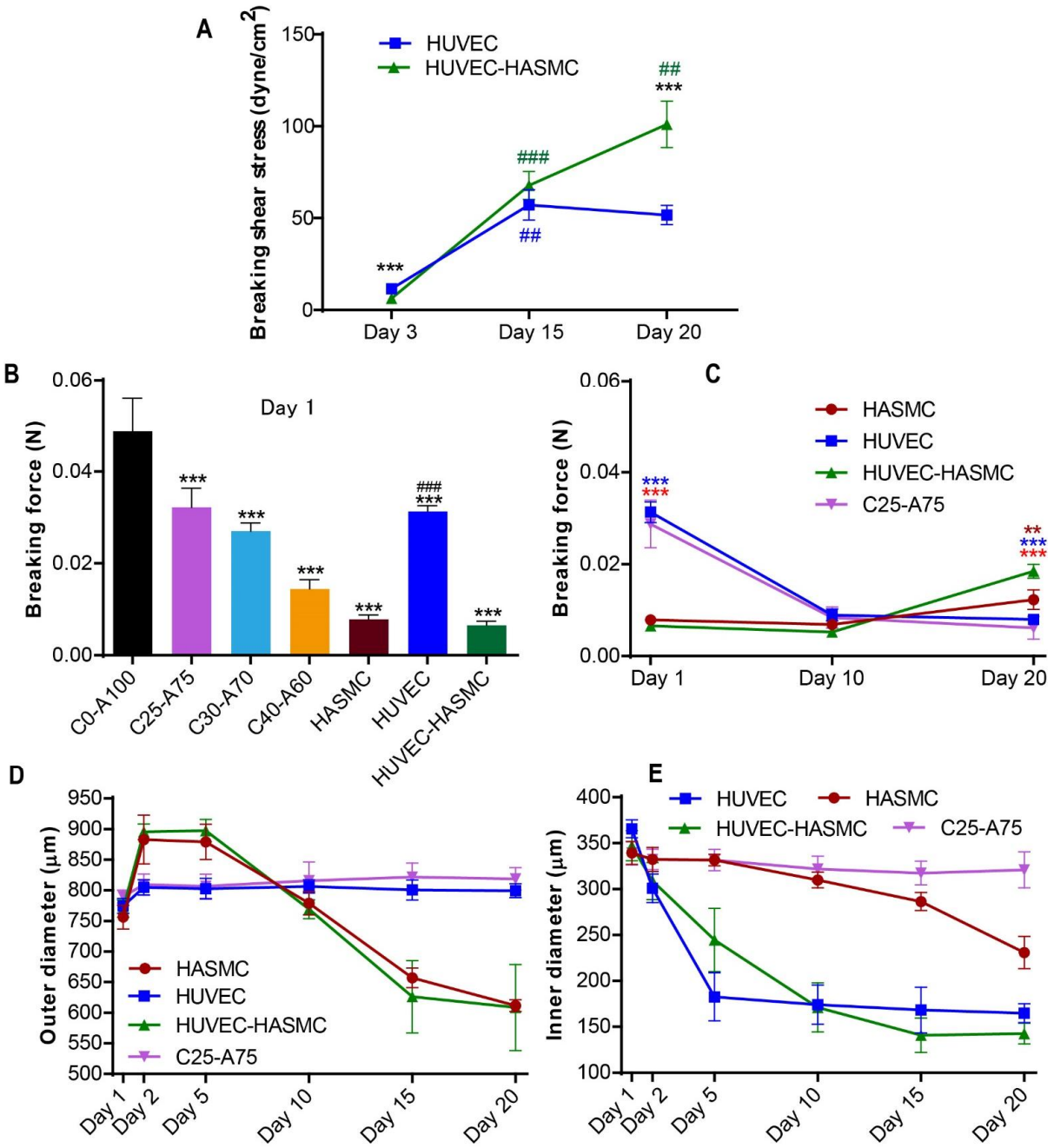

Figure 16: Mechanical strength testing. (a) The breaking shear-stress of the HUVEC–HASMC scaffold and the HUVEC core scaffold (*** $p < 0.001$, between the two type of scaffolds, n = 4), (## $0.001 < p < 0.01$, ### $p < 0.001$ compared with the previous day, n = 4). (b) The breaking force on day 1 (*** $p < 0.001$, compared with C0-A100, n = 5), (### $p < 0.001$, comparing the HUVEC–HASMC scaffold with the HASMC scaffold and the HUVEC scaffold, n = 5). (c) The breaking force with respect to the culture time (** $0.001 < p < 0.01$, ***$p < 0.001$, comparing the HUVEC–HASMC scaffold with the HASMC scaffold, the

HUVEC scaffold, and the cell-less scaffold, n = 5). (d) Changes in the outer diameter for up to 20 days. (e) Changes in the inner diameter for up to 20 days.

The axial breaking force of the collagen–alginate scaffolds was measured using a device that was designed based on [33]. Briefly, The measuring device comprised a moving part (a 5 cm long glass tube with a diameter of 1000 μm), and a sensing wire (a piano wire with a diameter of 500 μm or a 6 cm long glass capillary with a diameter of 164.4 μm). Glue was used to secure the scaffold sample between the sensing wire and the moving component. The entire system, including the scaffold sample, was soaked in deionized water for 10 minutes prior to pulling the moving part, and then measured in the deionized water. Equation 3 was used to determine the applied force (F):

$$F = k \times \Delta x \qquad \text{(Equation 3)}$$

where k was the spring constant (3.589754 N/m for the piano wire and 0.0065462 N/m for the glass tube), and Δx was the deformation of the sensing wire. Based on the vertical displacement (Δx') caused by 10 different weights, the spring constants of the piano wire and the glass capillary were determined. The average spring constants were then determined using a modified version of equation 3 as follows:

$$k = \frac{g \times m}{\Delta x'} \qquad \text{(Equation 4)}$$

where g, m, Δx' are gravitational acceleration, weight, and the vertical displacement, respectively.

On day 1, the breaking force of the cell-less scaffold and the cell-laden scaffold is compared in Figure 9b. The breaking point of the cell-less scaffold dropped as the collagen ratio rose. The HUVEC core scaffold and the cell-less scaffold had equivalent values when using the same hydrogel ratio (collagen:alginate at 25:75). The HUVEC–HASMC scaffold and the HASMC

scaffold, on the other hand, were only half as strong as the HUVEC core scaffold. $CaCl_2$ was pumped in as the core material for the HASMC scaffold while the HUVEC core and HUVEC–HASMC scaffolds were made with a combination of HUVECs and collagen as the core material.

The cell-laden scaffold's breaking force varied over time (Figure 16c). The breaking force of the HUVEC core scaffold and the cell-free scaffold reduced by less than half on day 10 compared to day 1, and the results were statistically equivalent on day 20. The breaking force of the HASMC shell and the HUVEC–HASMC scaffold was opposite, with no significant change between day 1 and day 10. Nevertheless, the breaking force of the HUVEC–HASMC scaffold had grown substantially by day 20. In comparison to a monoculture, the co-culture of HUVECs and HASMCs may generate a tougher ECM.

The ID and OD of the tubular scaffolds were measured using bright-field and fluorescent pictures throughout the culture period. The OD tendency of the HASMC shell layer scaffold and the HUVEC–HASMC scaffold was comparable (Figure 16d). They swelled on days 2 and 5, then started to contract drastically on day 10. However, the HUVEC core scaffold's OD showed a small increase over that time. The OD change seemed to be caused by the HASMC in the shell layer, while the HUVEC core was apparently the key factor in the ID difference. On days 2 and 5, the ID of the HUVEC core scaffold and the HUVEC–HASMC scaffold dropped faster than that of the HASMC shell layer scaffold (Figure 16e).

2.3.9 Angiogenesis

The HUVEC core and HUVEC–HASMC scaffolds were grown without growth factor (GF) supplement and buried within type I collagen matrices to evaluate the impact of HUVEC–HASMC co-culture on HUVEC angiogenesis. In a cell culture plate (35 mm diameter), a two-millilitre mixture of 3 mg/mL type I collagen and GF-free co-culture media (2:1 ratio) covered the cell-laden scaffolds. After that, for gelation the collagen dish was incubated for 45 minutes at 37 °C

with 5% CO_2. For up to 15 days, the scaffolds within the collagen dish were grown in 1.5 mL of fresh GR-free media, which was replaced every 24 hours. To check for CD31 protein expression, the sprouting scaffold was stained with CD31 monoclonal antibody (JC/70A) using the same technique as ZO-1 staining.

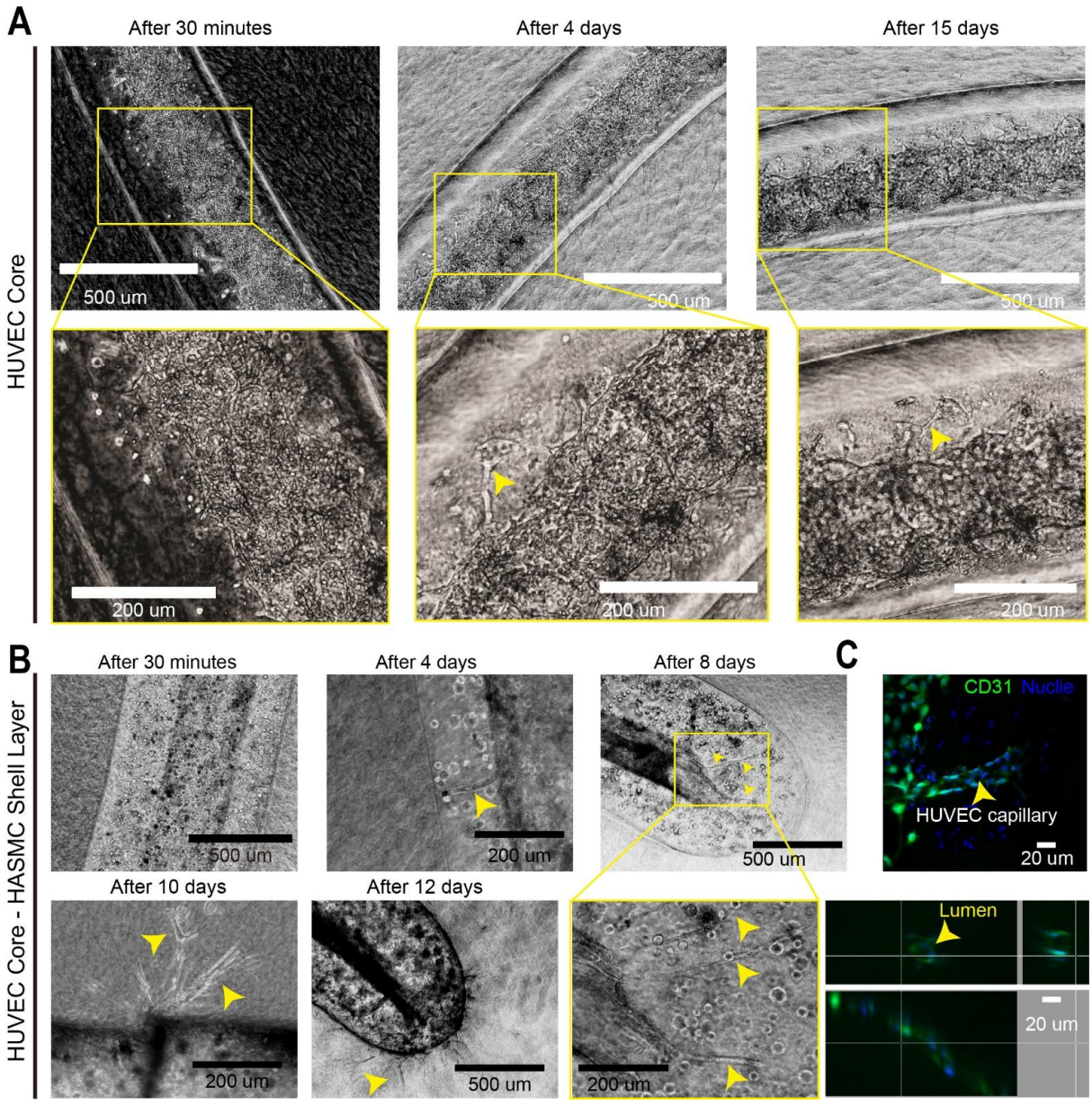

Figure 17: Angiogenesis within the collagen matrices (yellow arrows indicate cell sprouts). (a) The angiogenesis from the HUVEC scaffold was hardly detectable to day 15. (b) Cell sprouting and angiogenesis from the HUVEC–HASMC scaffold is clear. (c) Confocal immunostaining of the CD31 signal

showing the lumen structures of the HUVECs.

Sprouting from the core HUVECs was seen in both scaffolds, as illustrated in Figure 17. Until day 4, the HUVEC–HASMC scaffold had more fertile sprouting than the HUVEC core scaffold. Outside of the scaffold, the HUVEC–HASMC shell layer branched out to the collagen layer, but the HUVEC core scaffold did not appear to sprout into the cell-less shell layer. On day 10, a HUVEC (CD31) sprouting branch of the HUVEC–HASMC scaffold is shown in Figure 17c. The lumen of a 20-micrometer-diameter branch is visible in confocal microscope pictures (Figure 17c).

2.3.10 Gene expression

To investigate the effect of co-culture, gene expression was monitored for 15 days. On days 5, 10, and 15, the alginate hydrogel and collagen matrix encapsulating the seeded cells were degraded using alginate lyase (50 ng/L) and 0.05% trypsin EDTA, respectively. Total RNA was extracted according to the manufacturer's procedure using the Direct-zolTM RNA Mini-Prep Plus (Cat. number R2072, Zymo Research, USA). Then, using a High Capacity cDNA Reverse Transcription kit (Thermo Scientific, U.S.A.), cDNA was prepared. A real-time polymerase chain reaction (PCR) study using Luna Universal qPCR Master Mix (M3003, NEB, U.S.A.) was used to assess the gene expression level. An ABI 7500 Fast Real-Time PCR System (Applied Biosystems, U.S.A.) was used to monitor the PCR of the samples. To guarantee the single amplification of each gene, a melt curve analysis was conducted. The delta–delta technique was used to analyze the measured mRNA expression data, with beta-actin gene expression as a reference [53-55]. The gene-specific primers of genes including HASMC contractile marker genes (alpha-actin [38, 56] and smoothelin [38, 57, 58]), an angiogenic growth factor marker gene (VEGF) [59], and ECM protein

genes (collagen type I [38, 46], collagen type III [47], and collagen type IV [49]) are listed in Table 1. This experiment was carried out three times.

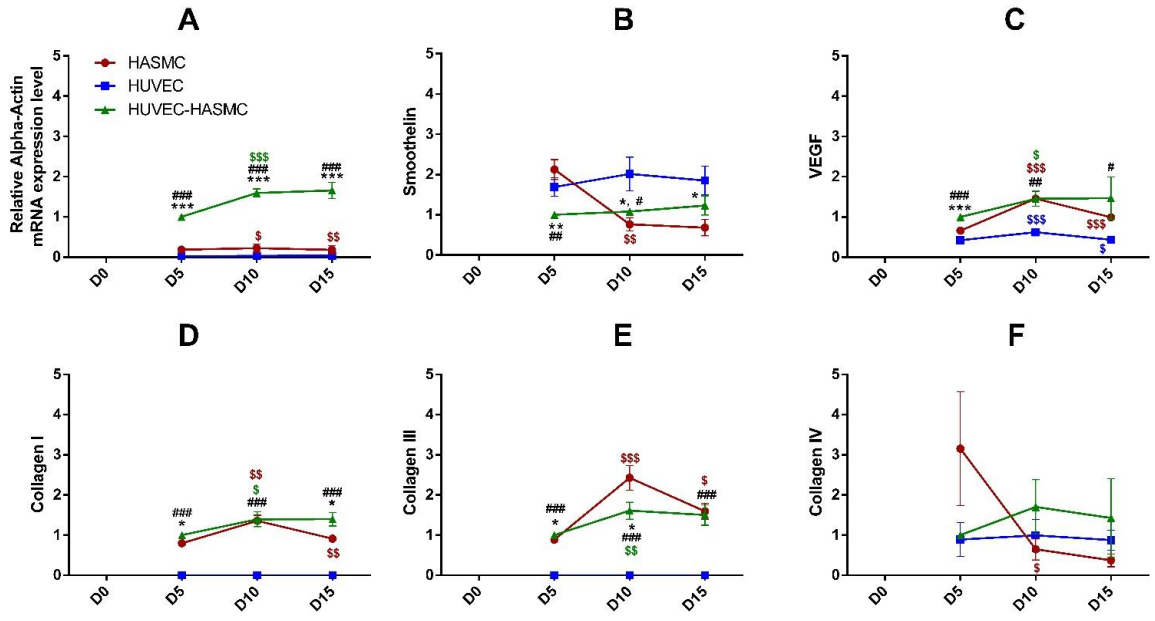

Figure 18: Gene expression. (a) Alpha-actin expression. (b) Smoothelin expression. (c) VEGF expression. (d) Collagen I expression. (e) Collagen III expression. (f) Collagen IV expression (* $0.01 < p < 0.05$, ** $0.001 < p < 0.01$, *** $p < 0.001$, between the HASMC scaffold and the HUVEC–HASMC scaffold, n = 3), (# $0.01 < p < 0.05$, ## $0.001 < p < 0.01$, ### $p < 0.001$, between the HUVEC scaffold and the HUVEC–HASMC scaffold, n = 3), ($ $0.01 < p < 0.05$, $$ $0.001 < p < 0.01$, $$$ $p < 0.001$, compared with the previous day, n = 3).

Effects of co-culture on HASMC differentiation

To see how co-culture influenced HASMC development, we looked at the expression of two contractile apparatus genes, alpha-actin and smoothelin [38]. The relative alpha-actin mRNA expression level in the HASMC only scaffolds increased by 20% on day 10 compared to day 5, then dropped substantially by day 15. (Figure 18a). The alpha-actin level in the HUVEC–HASMC scaffold was considerably greater on day 10 than on day 5, although it changed only little from that on day 15. During those 15 days, the HUVEC only scaffold exhibited almost

no alpha-actin expression. On all three days (days 5, 10, and 15), the alpha-actin level in the co-cultured HUVEC–HASMC scaffold was greater than in the other two hydrogels (p 0.001). The smoothelin expression peaked on day 5 in the HASMC-only scaffolds before rapidly declining (Figure 18b). The HUVEC only scaffold's smoothelin level fluctuated insignificantly. The smoothelin level in the HUVEC–HASMC scaffold did not vary substantially at any time period. As a result, determining the effect of co-culture on smoothelin was a challenge.

Effects of co-culture on HUVEC angiogenesis

The angiogenic factor VEGF promotes the creation of new blood vessels [60]. Its normal purpose is to stimulate new blood vessel formation during embryonic development (vasculogenesis) or new blood vessel growth from pre-existing ones (angiogenesis) [61]. To assess the influence of co-culture on HUVEC angiogenesis, the amount of VEGF gene expression was evaluated. The VEGF level in the HASMC only scaffold peaked on day 10 and subsequently dropped considerably by day 15 (Figure 18c). During the 15-day period, the HUVEC only scaffold had the lowest amount of VEGF among the three scaffolds, with little oscillation. The VEGF level in the HUVEC–HASMC scaffold was greatest on day 10 and thereafter stayed constant. On day 15, the HUVEC–HASMC scaffold had a significantly greater VEGF level than the monocellular scaffolds.

Effects of co-culture on ECM production

Three ECM genes: Collagen I, collagen III, and collagen IV were tested to see how co-culture influenced ECM synthesis. Such collagens can be found in the skin, lungs, intestinal wall, and blood vessel’s innermost membranes [46, 47, 49]. The expression levels of these three collagen genes in the HUVEC–HASMC scaffold followed a similar tendency: they rose until day 10 and then stayed constant (Figure 18d–f). The levels of collagen I and III in the HASMC only scaffold followed a similar pattern: they peaked on day 10 and then dropped

considerably on day 15. The collagen III expression had a greater peak value than that of collagen I in the HASMC only scaffold. The collagen I and II genes were not found in the HUVEC-only scaffold.

The expression of collagen IV gene exhibited a more complex pattern than the other collagens (Figure 18f). The collagen IV level in the HUVEC–HASMC scaffold peaked on day 10 and subsequently remained constant. Collagen IV peaked on day 5, dropped dramatically on day 10, and subsequently stayed unaltered in the HASMC only scaffold. On day 5, the collagen IV level in the HUVEC only scaffold followed the same tendency as the HUVEC–HASMC scaffold, but thereafter fluctuated insignificantly on days 10 and 15.

2.4 Discussion

We used a microfluidic-based nozzle and a combination of type I collagen and sodium alginate to print a free-standing HUVEC-HASMC coaxially layered scaffold without ultraviolet light illumination. Our printed structure comprised an endothelial lumen structure surrounded by elonging SMCs. This structure was similar to human native blood vessels. We also demonstrated and assessed its perfusability and angiogenesis.

Due to their tuneable biocompatibility and biodegradability, collagen-alginate hydrogels have been widely utilized in wound healing [62, 63] and bioprinting [64]. Specific peptide sequences in type I collagen can be recognized by cell surface receptors as a substrate for cell adhesion. Despite the fact that the sodium alginate polymeric backbone lacks an intrinsic cell-binding component, it can be utilized to improve the mechanical characteristics of a gel. The ratio of type I collagen in the blended hydrogel had a significant impact on cell spread over three days (Figure 4b). In addition, the inclusion of type I collagen in the sodium alginate improved cell adherence and cell culture media diffusion into the mixed hydrogel scaffold's deeper layers [65, 66]. The core-shell formation was

hampered when the collagen ratio in the mixed hydrogel was more than 40%. As a result, we used a 25:75 ratio for the collagen and alginate blend in this study. Crosslinking cation diffusion from the interior of the shell layer to the outside was produced by the $CaCl_2$ in the core material [67, 68]. During 3D macro-scaffold bioprinting, this diffusion gradient facilitated fibre–fibre attachment [69]. The core-shell scaffold was produced uniformly and without clogging from the outlet (Figure 6d–e), allowing for meter-long scaffold formation. The core-shell scaffold was generated with variable wall thickness when the core flow rate was changed. At a core flow rate of 0.01 mL/min, the wall thickness was approximately 350 µm. When the shell flow rate was kept at 0.7 mL/min, the thickness was decreased to 190 µm at a core flow rate of 0.10 mL/min (Figure 19). This control of wall thickness was used to simulate the varied wall thicknesses observed in human venous and arterial vessels [70].

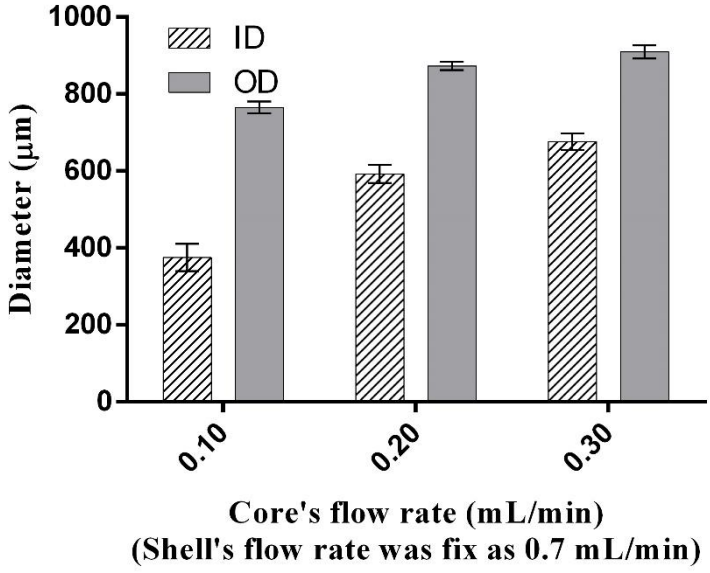

Figure 19: Inner and outer diameter changes when the shell's flow rate was fixed at 0.7 mL/min and the core's flow rate ranged from 0.01 mL/min to 0.3 mL/min (sample size n = 10 from 2 experiments).

HUVECs were encapsulated in 3 mg/mL type I collagen as the core material, forming a perfusable channel along the axial direction of the scaffold (Figure 11a–b). The original collagen matrix was replaced by newly secreted ECM [33] as the cells developed, resulting in a lumen structure (Figure 13) and increased toughness (Figure 16a–c) [71]. The HUVECs migrated six hours after scaffold formation and self-organized into a lumen monolayer (Figure 11a–b, Figure 13), with a density of 1.7×10^7 cells/mL. The ZO-1 also exhibited tight cell–cell connections (Figure 11c). A coarse lumen shape was seen until day 5 with a reduced density (3.5×10^6 cells/mL) of HUVECs (Figure 11a–b, Figure 13). Given the structural and cell type similarities between the findings of L'Heureux et al. [72] and Gao *et al.* [30], our fabicated HUVEC–HASMC scaffold may be feasible to inhibit platelet adhesion and blood clotting as such results.

Various reported researches have looked at the impact of a diffusion-limited environment, which occurs when cells are seeded deeper than the normal diffusion distance of nutrients and oxygen [17, 32, 73]. The greatest natural diffusion distance is about 200 μm, thus perfusable networks are necessary to feed nutrients to every living cells [13, 73]. Some endothelialized perfusable networks were developed on microfluidic chips to investigate physiological and biofunctional properties of microvascular tissues [17, 74-76]. Because these networks are securely connected as microscale patterns on a polymeric or glass substrate, they cannot be harvested for implantation or other free-standing tests. Without the use of a microfluidic chip, our perfusable, cell-laden scaffold was extruded in a free-standing form (Figure 6d–f, Figure 20) and then mounted to a medium pumping system using an in-house designed connection (Figure 15). During perfusion with flow rates less than 0.1 mL/min, the structural integrity of the continuous hollow cell scaffolds was preserved (Figure 15e–g). In our previous publication, mouse fibroblasts (NIH/3T3) inside an alginate scaffold increased their proliferation, confluence, and vitality when we applied a cell culture medium pumping condition [32]. With a flow rate of 0.02 mL/min and an

in-house connector, a secure connection was maintained for up to 14 days in the heartbeat mimicking pumping condition and for 12 days in the continuous pumping condition. Despite the tight connection between the medium pump and the 3T3-laden scaffold, the scaffold may be destroyed by an external shock during the handling procedure since the cell-laden scaffolds floated inside the cell media. In this work, we placed a small glass capillary in the middle of the cell-laden scaffold (Figures 15a, d, and e), which decreased the impact of shear stress on the shell layer of the scaffold. As a result of this design, the medium pumping system has a stable and long-term link. During handling, the collagen matrix also kept the scaffold steady and shielded it from external disturbance (Figure 15b). This suggested technique might be used to further investigate physiological processes of human blood vessels including lumen morphogenesis [17, 77], angiogenesis [74], hemodynamic resistance, and immune responses.

Over time, the mechanical strenth of the cell scaffold was changed. In terms of shear stress resistance, the HUVEC core scaffold and the HUVEC–HASMC scaffold had opposing results (Figure 16a). The HUVEC–HASMC scaffold's shear stress resistance was initially lower than the HUVEC scaffold's, but by day 20, it had grown to 103 dyne/cm^2. Indeed, actin filaments resist cell stretching and shortening, according to Nagayama's findings [78]. The greater alpha-actin level detected in the HUVEC–HASMC scaffold on day 20 (Figure 18a) appears to be involved in its high shear stress durability, given their involvement in muscle function (Figure 16a).

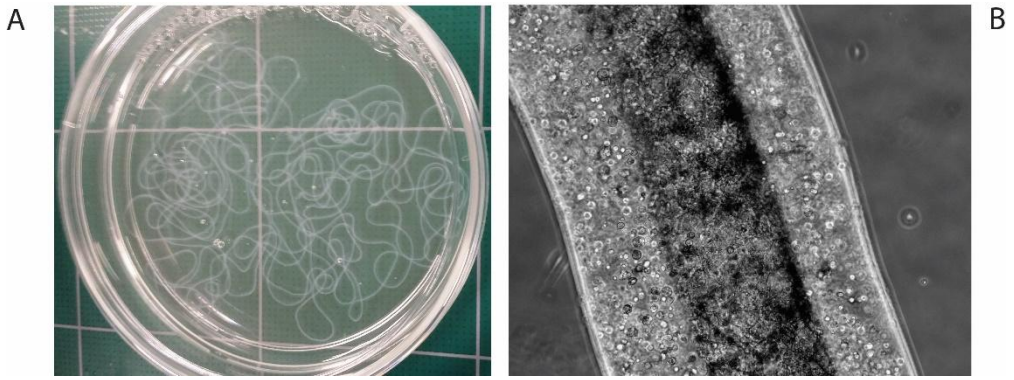

Figure 20: Free-standing scaffolds (a) Co-culture scaffolds in PBS on day 3. (b) Co-culture scaffold on a glass slide on day 3.

Importantly, the HUVEC core scaffold showed comparable toughness over time to the cell-free scaffold (C25-A75) (Figure 16b–c). On the other hand, on day 1, the HASMC and HUVEC–HASMC scaffolds were much less tough than the HUVEC core scaffold. By day 20, the two HASMC-laden scaffolds had outperformed the HUVEC core scaffold in terms of toughness (Figure 16c). The scaffolds are assumed that their HASMC shell layer shrunk to cause the wall became denser and more durable.

HASMC and HUVEC–HASMC scaffold OD alterations followed a similar tendency (Figure 16d). On day 1, the OD was around 750 μm, peaked on day 5, and subsequently dropped below 750 μm on day 20. The OD of the HUVEC scaffold, on the other hand, did not alter much after day 1. We deduced that HASMCs played an important role in scaffold shrinking since no HASMCs were found in the shell layer of the HUVEC scaffold.

Similar tendencies were seen in the ID of HUVEC-laden scaffolds (the HUVEC core scaffold and the HUVEC–HASMC scaffold) (Figure 16e). When compared to the ID of the HUVEC-free scaffold, the ID was around 350 μm on day 1 and subsequently quickly dropped on days 2 and 5. (i.e., the HASMC shell layer scaffold). The ID difference between the HUVEC-laden and HUVEC-less scaffolds was about 100 μm on day 20. As a result, the ID changes looked to be caused by the HUVEC core.

CD31 marker has been popularly used to show the stratification od ECs and SMCs [79-81]. The presence of CD31 (green) revealed the formation of small neo-vessels under the confocal microscope, as shown in Figure 17c. Figure 17a–b showed that the HUVEC–HASMC scaffold had much higher cell sprouting than the HUVEC core scaffold. Furthermore, the HUVEC core and HASMC shell layer sprang out of the scaffold and into the collagen matrix. The HUVEC core scaffold, on the other hand, did not sprout to the cell-less shell layer when it was far away from the buried collagen outside the scaffold. The VEGF level in the HUVEC–HASMC scaffold was greater than in the HUVEC scaffold, which might explain such discrepancy (Figure 18c). Growth factors including PDGF, VEGF, and TGF- were demonstrated to promote angiogenic morphogenesis of ECs, according to previous studies [74, 76, 82, 83]. Indeed, co-cultured SMCs and ECs secreted more PDGF-BB and TGF-1 than SMC monocultures, according to Liu *et al.* [38]. Our technique appears to have recapitulated the angiogenesis of native vasculature, as evidenced by these combined observations.

The contractile apparatus of SMCs is mostly composed of alpha-actin [84]. PDGF-BB, on the other hand, suppresses the expression of several CArG-containing SMC marker genes, such as alpha-actin [85]. Because PDGF-BB secretion was observed as early as day 4 in Liu's co-culture experiments, the maximal alpha-actin level was measured on day 10, which is consistent with our findings (Figure 18a). Smoothelin's expression was unaffected by PDGF-BB because it lacks a myocardin-SRF-dependent regulatory mechanism (Figure 18b).

In a native blood vessel, SMCs are found in ECM components such as ollagens I, III, and V, elastin, and proteoglycans which are primary elements of tunica media. In the meanwhile, the innermost membrane is made up of an EC monolayer and a basal lamina made up of mesh-like type IV collagen and adhesion molecules [86]. We demonstrated that collagens I and II were not epressed in the HUVEC scaffold (Figure 18d–e). The difference in collagen type

I expression between the HUVEC–HASMC scaffold and the HASMC scaffold on day 10 was not significant, which is consistent with prior studies [38, 87]. In both scaffolds that containing HASMCs, collagen type III expression peaked on day 10 (Figure 18e). On day 10, the collagen type IV level in the HUVEC–HASMC scaffold rose, but it began to drop in the HUVEC core scaffold on day 5 (Figure 18f).

Chapter 3:
Conclusion

The dissertation achieved remarkable results as the early objectives. We developed a microfluidic nozzle that was able to continuously print the structural and functional blood vessels at the microscopic scale. Layered co-culture of HUVECs and HASMCs within collagen-based hydrogels using our developed method enhanced cell differentiation, ECM secretion, angiogenesis, toughness, and durability. With potential printability, our technique could be further applied to the volumetric printing of vascularised tissues.

Besides obtained achievements, the dissertation still contains several limitations that need to be addressed. The double-layered blood vessel needs to be cultured under a physiological hemodynamic condition (cell culture medium pumping condition) for a long time (> 24 hours). This configuration would allow mimicking heart pressure pumping that is necessary to sufficiently supply nutrients to cells and form a smooth monolayer of endothelial cells. In addition, sodium alginate is not a component of ECM thus it is insufficient to reconstruct a 3D microenvironment for cellular growth. Hence, the sodium alginate ratio should be reduced in the bio-ink for the shell material to for the vessel.

REFERENCES

[1] C. E. Riva, J. E. Grunwald, S. H. Sinclair, and B. L. Petrig, "Blood velocity and volumetric flow rate in human retinal vessels," *Investigative ophthalmology & visual science,* vol. 26, no. 8, pp. 1124-32, 1985. [Online]. Available: http://www.ncbi.nlm.nih.gov/pubmed/4019103%5Cnhttp://www.iovs.org/cgi/pmidlookup?view=long&pmid=4019103%5Cnhttp://www.iovs.org/content/26/8/1124.short%5CnAll Papers/R/Riva et al. 1985 - Blood velocity and volumetric flow rate in human retinal vessels.pdf.

[2] Y. K. Tao, K. M. Kennedy, and J. a. Izatt, "Velocity-resolved 3D retinal microvessel imaging using single-pass flow imaging spectral domain optical coherence tomography," *Optics express,* vol. 17, no. 5, pp. 4177-4188, 2009, doi: 10.1364/OE.17.004177.

[3] Y. Wang, B. A. Bower, J. A. Izatt, O. Tan, and D. Huang, "In vivo total retinal blood flow measurement by Fourier domain Doppler optical coherence tomography," *Journal of Biomedical Optics,* vol. 12, no. 4, pp. 041215-041215, 2007, doi: 10.1117/1.2772871.

[4] W. M. Haschek, C. G. Rousseaux, and M. A. Wallig, "Chapter 12 - Cardiovascular and Skeletal Muscle Systems," in *Fundamentals of Toxicologic Pathology (Second Edition)*, W. M. Haschek, C. G. Rousseaux, and M. A. Wallig Eds. San Diego: Academic Press, 2010, pp. 319-376.

[5] D. Van Thuy, D. Thao Thi, C. Hwang Ho, B. Sung Hoon, and K. Kyo-in, "Coaxial printing of double-layered and free-standing blood vessel analogues without ultraviolet illumination for high-volume vascularised tissue," *Biofabrication,* 2020, doi: 10.1088/1758-5090/abafc6.

[6] A. Roberts, *The Complete Human Body*. DK, 2010.

[7] A. S. Hafez and M. R. Lesk, "9 - Role of Ocular Blood Flow in the Pathogenesis of Glaucoma," in *Glaucoma (Second Edition)*, T. M.

Shaarawy, M. B. Sherwood, R. A. Hitchings, and J. G. Crowston Eds.: W.B. Saunders, 2015, pp. 88-97.

[8] A. K. A. Ronald A. Bergman, Paul M. Heidger. "Anatomy Atlases: Section 8: Cardiovascular System." https://www.anatomyatlases.org/MicroscopicAnatomy/Section08/Section08.shtml (accessed 2019 Oct 17.

[9] M. R. V. LadyofHats, "Circulatory System," ed. Wikipedia, 2021.

[10] HRSA. "Organ Donation Statistics." https://www.organdonor.gov/learn/organ-donation-statistics (accessed 2021).

[11] D. L. America. "Organ, Eye and Tissue Donation Statistics." https://www.donatelife.net/statistics/ (accessed 2021).

[12] J. Litowczenko, M. J. Woźniak-Budych, K. Staszak, K. Wieszczycka, S. Jurga, and B. Tylkowski, "Milestones and current achievements in development of multifunctional bioscaffolds for medical application," *Bioactive Materials,* vol. 6, no. 8, pp. 2412-2438, 2021/08/01/ 2021, doi: 10.1016/j.bioactmat.2021.01.007.

[13] P. Carmeliet and R. K. Jain, "Angiogenesis in cancer and other diseases," *Nature,* vol. 407, no. 6801, pp. 249-257, 2000/09/01 2000, doi: 10.1038/35025220.

[14] M. Lovett, K. Lee, A. Edwards, and D. L. Kaplan, "Vascularization Strategies for Tissue Engineering," *Tissue Engineering Part B: Reviews,* vol. 15, no. 3, pp. 353-370, 2009/09/01 2009, doi: 10.1089/ten.teb.2009.0085.

[15] G. Gao, B. S. Kim, J. Jang, and D.-W. Cho, "Recent Strategies in Extrusion-Based Three-Dimensional Cell Printing toward Organ Biofabrication," *ACS Biomaterials Science & Engineering,* vol. 5, no. 3, pp. 1150-1169, 2019/03/11 2019, doi: 10.1021/acsbiomaterials.8b00691.

[16] J. S. Miller, K. R. Stevens, M. T. Yang, B. M. Baker, D.-H. T. Nguyen, D. M. Cohen, E. Toro, A. A. Chen, P. A. Galie, X. Yu, R. Chaturvedi, S. N. Bhatia, and C. S. Chen, "Rapid casting of patterned vascular networks for perfusable engineered three-dimensional tissues," *Nature Materials,* vol. 11, p. 768, 07/01/online 2012, doi: 10.1038/nmat3357.

[17] V. K. Lee, D. Y. Kim, H. Ngo, Y. Lee, L. Seo, S.-S. Yoo, P. A. Vincent, and G. Dai, "Creating perfused functional vascular channels using 3D bio-printing technology," *Biomaterials,* vol. 35, no. 28, pp. 8092-8102, 2014/09/01/ 2014, doi: 10.1016/j.biomaterials.2014.05.083.

[18] L. E. Bertassoni, M. Cecconi, V. Manoharan, M. Nikkhah, J. Hjortnaes, A. L. Cristino, G. Barabaschi, D. Demarchi, M. R. Dokmeci, Y. Yang, and A. Khademhosseini, "Hydrogel bioprinted microchannel networks for vascularization of tissue engineering constructs," *Lab on a Chip,* 10.1039/C4LC00030G vol. 14, no. 13, pp. 2202-2211, 2014, doi: 10.1039/C4LC00030G.

[19] W. Wu, A. DeConinck, and J. A. Lewis, "Omnidirectional Printing of 3D Microvascular Networks," *Advanced Materials,* vol. 23, no. 24, pp. H178-H183, 2011/06/24 2011, doi: 10.1002/adma.201004625.

[20] K. Peters and F. M. Richards, "Chemical cross-linking: reagents and problems in studies of membrane structure," *Annu Rev Biochem,* vol. 46, pp. 523-51, 1977, doi: 10.1146/annurev.bi.46.070177.002515.

[21] E. N. Christiansen and E. Kvamme, "Effects of Thermal Treatment on Mitochondria of Brain, Liver and Ascites Cells," *Acta Physiologica Scandinavica,* vol. 76, no. 4, pp. 472-484, 1969/08/01 1969, doi: 10.1111/j.1748-1716.1969.tb04494.x.

[22] O. W. Kaufmann, L. G. Harmon, O. C. Pail Thorp, and I. J. Pflug, "Effect of heat treatment on the growth of surviving cells," (in eng), *Journal of bacteriology,* vol. 78, no. 6, pp. 834-838, 1959. [Online]. Available: https://www.ncbi.nlm.nih.gov/pmc/articles/PMC290640/.

[23] Y. Zhang, Y. Yu, and I. T. Ozbolat, "Direct Bioprinting of Vessel-Like Tubular Microfluidic Channels," (in eng), *J Nanotechnol Eng Med,* vol. 4, no. 2, pp. 0210011-0210017, 2013, doi: 10.1115/1.4024398.

[24] A. K. Miri, I. Mirzaee, S. Hassan, S. Mesbah Oskui, D. Nieto, A. Khademhosseini, and Y. S. Zhang, "Effective bioprinting resolution in tissue model fabrication," *Lab on a Chip,* 10.1039/C8LC01037D vol. 19, no. 11, pp. 2019-2037, 2019, doi: 10.1039/C8LC01037D.

[25] Q. Pi, S. Maharjan, X. Yan, X. Liu, B. Singh, A. M. van Genderen, F. Robledo-Padilla, R. Parra-Saldivar, N. Hu, W. Jia, C. Xu, J. Kang, S. Hassan, H. Cheng, X. Hou, A. Khademhosseini, and Y. S. Zhang, "Digitally Tunable Microfluidic Bioprinting of Multilayered Cannular Tissues," *Advanced Materials,* vol. 30, no. 43, p. 1706913, 2018, doi: 10.1002/adma.201706913.

[26] T. Bonura and K. C. Smith, "Enzymatic production of deoxyribonucleic acid double-strand breaks after ultraviolet irradiation of Escherichia coli K-12," *Journal of Bacteriology,* vol. 121, no. 2, pp. 511-517, 1975. [Online]. Available: https://jb.asm.org/content/jb/121/2/511.full.pdf.

[27] M. Y. Roleda, C. Wiencke, and U. H. Lüder, "Impact of ultraviolet radiation on cell structure, UV-absorbing compounds, photosynthesis, DNA damage, and germination in zoospores of Arctic Saccorhiza dermatodea," *Journal of Experimental Botany,* vol. 57, no. 14, pp. 3847-3856, 2006, doi: 10.1093/jxb/erl154.

[28] J. Moan and M. J. Peak, "Effects of UV radiation on cells," *Journal of Photochemistry and Photobiology B: Biology,* vol. 4, no. 1, pp. 21-34, 1989/10/01/ 1989, doi: 10.1016/1011-1344(89)80099-5.

[29] G. Gao, J. H. Lee, J. Jang, D. H. Lee, J. S. Kong, B. S. Kim, Y. J. Choi, W. B. Jang, Y. J. Hong, S. M. Kwon, and D. W. Cho, "Tissue Engineered Bio□Blood□Vessels Constructed Using a Tissue□Specific Bioink and 3D Coaxial Cell Printing Technique: A Novel Therapy for Ischemic Disease,"

Advanced Functional Materials, vol. 27, no. 33, 2017, doi: 10.1002/adfm.201700798.

[30] G. Gao, J. Y. Park, B. S. Kim, J. Jang, and D.-W. Cho, "Coaxial Cell Printing of Freestanding, Perfusable, and Functional In Vitro Vascular Models for Recapitulation of Native Vascular Endothelium Pathophysiology," *Advanced Healthcare Materials,* vol. 7, no. 23, p. 1801102, 2018/12/01 2018, doi: 10.1002/adhm.201801102.

[31] V. T. Duong, T. T. Dang, Y. Lee, C. T. Nguyen, H. L. Phan, D. Shin, Y. Lee, H. Park, H. Lee, H. Son, H. Jang, S. Oh, S. H. Back, C. Hwang, and K. K. a, "Cell Attachment on Inside-Outside Surface and Cell Encapsulation in Wall of Microscopic Tubular Scaffolds for Vascular Tissue-Like Formation," in *2018 40th Annual International Conference of the IEEE Engineering in Medicine and Biology Society (EMBC)*, 18-21 July 2018 2018, pp. 4198-4201, doi: 10.1109/EMBC.2018.8513248.

[32] V. T. Duong, T. T. Dang, J. P. Kim, K. Kim, H. Ko, C. H. Hwang, and K. I. Koo, "Twelve-day medium pumping into tubular cell-laden scaffold using a lab-made PDMS connector," *Eur Cell Mater,* vol. 38, pp. 1-13, Jul 23 2019, doi: 10.22203/eCM.v038a01.

[33] H. Onoe, T. Okitsu, A. Itou, M. Kato-Negishi, R. Gojo, D. Kiriya, K. Sato, S. Miura, S. Iwanaga, K. Kuribayashi-Shigetomi, Y. T. Matsunaga, Y. Shimoyama, and S. Takeuchi, "Metre-long cell-laden microfibres exhibit tissue morphologies and functions," *Nature Materials,* Article vol. 12, p. 584, 03/31/online 2013, doi: 10.1038/nmat3606.

[34] D. Kefallinou, M. Grigoriou, D. T. Boumpas, E. Gogolides, and A. Tserepi, "Fabrication of a 3D microfluidic cell culture device for bone marrow-on-a-chip," *Micro and Nano Engineering,* vol. 9, p. 100075, 2020/11/01/ 2020, doi: 10.1016/j.mne.2020.100075.

[35] P. F. Costa, H. J. Albers, J. E. A. Linssen, H. H. T. Middelkamp, L. van der Hout, R. Passier, A. van den Berg, J. Malda, and A. D. van der Meer,

"Mimicking arterial thrombosis in a 3D-printed microfluidic in vitro vascular model based on computed tomography angiography data," *Lab on a Chip,* 10.1039/C7LC00202E vol. 17, no. 16, pp. 2785-2792, 2017, doi: 10.1039/C7LC00202E.

[36] P. Allen, J. Melero-Martin, and J. Bischoff, "Type I collagen, fibrin and PuraMatrix matrices provide permissive environments for human endothelial and mesenchymal progenitor cells to form neovascular networks," *Journal of Tissue Engineering and Regenerative Medicine,* vol. 5, no. 4, pp. e74-e86, 2011/04/01 2011, doi: 10.1002/term.389.

[37] A. BioMatrix. "Collagen Concentration vs Gel Stiffness." https://advancedbiomatrix.com/collagenconcentrationvideo.html (accessed 2021).

[38] Y. Liu, S. Rayatpisheh, S. Y. Chew, and M. B. Chan-Park, "Impact of Endothelial Cells on 3D Cultured Smooth Muscle Cells in a Biomimetic Hydrogel," *ACS Applied Materials & Interfaces,* vol. 4, no. 3, pp. 1378-1387, 2012/03/28 2012, doi: 10.1021/am201648f.

[39] G. K. Owens, M. S. Kumar, and B. R. Wamhoff, "Molecular Regulation of Vascular Smooth Muscle Cell Differentiation in Development and Disease," *Physiological Reviews,* vol. 84, no. 3, pp. 767-801, 2004, doi: 10.1152/physrev.00041.2003.

[40] S. Au - Meghezi, D. G. Au - Seifu, N. Au - Bono, L. Au - Unsworth, K. Au - Mequanint, and D. Au - Mantovani, "Engineering 3D Cellularized Collagen Gels for Vascular Tissue Regeneration," *JoVE,* no. 100, p. e52812, 2015/06/16/ 2015, doi: doi:10.3791/52812.

[41] R. J. Powell, J. Hydowski, O. Frank, J. Bhargava, and B. E. Sumpio, "Endothelial Cell Effect on Smooth Muscle Cell Collagen Synthesis," *Journal of Surgical Research,* vol. 69, no. 1, pp. 113-118, 1997/04/01/ 1997, doi: 10.1006/jsre.1997.5045.

[42] H.-Q. Wang, L. Bai, B.-R. Shen, Z.-Q. Yan, and Z.-L. Jiang, "Coculture with endothelial cells enhances vascular smooth muscle cell adhesion and spreading via activation of β1-integrin and phosphatidylinositol 3-kinase/Akt," *European Journal of Cell Biology,* vol. 86, no. 1, pp. 51-62, 2007/01/17/ 2007, doi: 10.1016/j.ejcb.2006.09.001.

[43] S. Heydarkhan-Hagvall, G. Helenius, B. R. Johansson, J. Y. Li, E. Mattsson, and B. Risberg, "Co-culture of endothelial cells and smooth muscle cells affects gene expression of angiogenic factors," *Journal of Cellular Biochemistry,* vol. 89, no. 6, pp. 1250-1259, 2003, doi: 10.1002/jcb.10583.

[44] R. J. Powell, J. A. Carruth, M. D. Basson, R. Bloodgood, and B. E. Sumpio, "Matrix-specific effect of endothelial control of smooth muscle cell migration," *Journal of Vascular Surgery,* vol. 24, no. 1, pp. 51-57, 1996/07/01/ 1996, doi: 10.1016/S0741-5214(96)70144-1.

[45] M. F. Fillinger, L. N. Sampson, J. L. Cronenwett, R. J. Powell, and R. J. Wagner, "Coculture of Endothelial Cells and Smooth Muscle Cells in Bilayer and Conditioned Media Models," *Journal of Surgical Research,* vol. 67, no. 2, pp. 169-178, 1997/02/01/ 1997, doi: 10.1006/jsre.1996.4978.

[46] U. S. N. L. o. Medicine. "COL1A1 gene." https://ghr.nlm.nih.gov/gene/COL1A1 (accessed 09/17, 2019).

[47] U. S. N. L. o. Medicine. "COL3A1 gene." https://ghr.nlm.nih.gov/gene/COL3A1 (accessed 09/17, 2019).

[48] N. N. C. f. B. Information. "Standard Nucleotide BLAST." https://blast.ncbi.nlm.nih.gov/Blast.cgi#1780266030 (accessed.

[49] U. S. N. L. o. Medicine. "COL4A1 gene." https://ghr.nlm.nih.gov/gene/COL4A1 (accessed 09/17, 2019).

[50] K. Henriksen and M. A. Karsdal, "Chapter 1 - Type I Collagen," in *Biochemistry of Collagens, Laminins and Elastin*, M. A. Karsdal Ed.: Academic Press, 2016, pp. 1-11.

[51] L. Ning, H. Sun, T. Lelong, R. Guilloteau, N. Zhu, D. J. Schreyer, and X. Chen, "3D bioprinting of scaffolds with living Schwann cells for potential nerve tissue engineering applications," *Biofabrication,* vol. 10, no. 3, p. 035014, 2018/06/29 2018, doi: 10.1088/1758-5090/aacd30.

[52] A. Biotech. "Collagen Gel Preparation Protocol." https://www.youtube.com/watch?v=x3Rmj3ALoOI (accessed January 01, 2019).

[53] R. Mori, Q. Wang, K. D. Danenberg, J. K. Pinski, and P. V. Danenberg, "Both beta-actin and GAPDH are useful reference genes for normalization of quantitative RT-PCR in human FFPE tissue samples of prostate cancer," *Prostate,* vol. 68, no. 14, pp. 1555-60, Oct 1 2008, doi: 10.1002/pros.20815.

[54] M. Mani, D. T. Thao, B. C. Kim, U. H. Lee, D. J. Kim, S. H. Jang, S. H. Back, B. J. Lee, W. J. Cho, I.-S. Han, and J. W. Park, "DRG2 knockdown induces Golgi fragmentation via GSK3β phosphorylation and microtubule stabilization," *Biochimica et Biophysica Acta (BBA) - Molecular Cell Research,* vol. 1866, no. 9, pp. 1463-1474, 2019/09/01/ 2019, doi: 10.1016/j.bbamcr.2019.06.003.

[55] T. Dang, S. H. Jang, S. H. Back, J. W. Park, and I. S. Han, "DRG2 Deficiency Causes Impaired Microtubule Dynamics in HeLa Cells," *Mol Cells,* vol. 41, no. 12, pp. 1045-1051, Dec 31 2018, doi: 10.14348/molcells.2018.0129.

[56] N. L. o. Medicine. "ACTG2 gene." https://ghr.nlm.nih.gov/gene/ACTG2 (accessed 2019).

[57] N. C. f. B. Information. "SMTN smoothelin [Homo sapiens (human)]." https://www.ncbi.nlm.nih.gov/gene/6525 (accessed 2019).

[58] Uniprot. "UniProtKB - P53814 (SMTN_HUMAN)." https://www.uniprot.org/uniprot/P53814 (accessed 09/16, 2019).

[59] N. L. o. Medicine. "VEGFA gene." https://ghr.nlm.nih.gov/gene/VEGFA (accessed 2019.

[60] D. H. T. Nguyen, S. C. Stapleton, M. T. Yang, S. S. Cha, C. K. Choi, P. A. Galie, and C. S. Chen, "Biomimetic model to reconstitute angiogenic sprouting morphogenesis in vitro," *Proceedings of the National Academy of Sciences,* vol. 110, no. 17, pp. 6712-6717, 2013, doi: 10.1073/pnas.1221526110.

[61] B. Vailhé, D. Vittet, and J.-J. Feige, "In Vitro Models of Vasculogenesis and Angiogenesis," *Laboratory Investigation,* vol. 81, no. 4, pp. 439-452, 2001/04/01 2001, doi: 10.1038/labinvest.3780252.

[62] H. Xie, X. Chen, X. Shen, Y. He, W. Chen, Q. Luo, W. Ge, W. Yuan, X. Tang, D. Hou, D. Jiang, Q. Wang, Y. Liu, Q. Liu, and K. Li, "Preparation of chitosan-collagen-alginate composite dressing and its promoting effects on wound healing," *International Journal of Biological Macromolecules,* vol. 107, pp. 93-104, 2018/02/01/ 2018, doi: 10.1016/j.ijbiomac.2017.08.142.

[63] V. V. S. R. Karri, G. Kuppusamy, S. V. Talluri, S. S. Mannemala, R. Kollipara, A. D. Wadhwani, S. Mulukutla, K. R. S. Raju, and R. Malayandi, "Curcumin loaded chitosan nanoparticles impregnated into collagen-alginate scaffolds for diabetic wound healing," *International Journal of Biological Macromolecules,* vol. 93, pp. 1519-1529, 2016/12/01/ 2016, doi: 10.1016/j.ijbiomac.2016.05.038.

[64] X. Yang, Z. Lu, H. Wu, W. Li, L. Zheng, and J. Zhao, "Collagen-alginate as bioink for three-dimensional (3D) cell printing based cartilage tissue engineering," *Materials Science and Engineering: C,* vol. 83, pp. 195-201, 2018/02/01/ 2018, doi: 10.1016/j.msec.2017.09.002.

[65] C. Branco da Cunha, D. D. Klumpers, W. A. Li, S. T. Koshy, J. C. Weaver, O. Chaudhuri, P. L. Granja, and D. J. Mooney, "Influence of the stiffness of three-dimensional alginate/collagen-I interpenetrating networks on fibroblast biology," *Biomaterials,* vol. 35, no. 32, pp. 8927-8936, 2014/10/01/ 2014, doi: 10.1016/j.biomaterials.2014.06.047.

[66] R. Mahou, A. E. Vlahos, A. Shulman, and M. V. Sefton, "Interpenetrating Alginate-Collagen Polymer Network Microspheres for Modular Tissue Engineering," *ACS Biomaterials Science & Engineering,* vol. 4, no. 11, pp. 3704-3712, 2018/11/12 2018, doi: 10.1021/acsbiomaterials.7b00356.

[67] A. Blandino, M. Macías, and D. Cantero, "Formation of calcium alginate gel capsules: Influence of sodium alginate and CaCl2 concentration on gelation kinetics," *Journal of Bioscience and Bioengineering,* vol. 88, no. 6, pp. 686-689, 1999/01/01/ 1999, doi: 10.1016/S1389-1723(00)87103-0.

[68] J. M. Sonego, P. R. Santagapita, M. Perullini, and M. Jobbágy, "Ca(ii) and Ce(iii) homogeneous alginate hydrogels from the parent alginic acid precursor: a structural study," *Dalton Transactions,* 10.1039/C6DT00321D vol. 45, no. 24, pp. 10050-10057, 2016, doi: 10.1039/C6DT00321D.

[69] W. Liu, Z. Zhong, N. Hu, Y. Zhou, L. Maggio, A. K. Miri, A. Fragasso, X. Jin, A. Khademhosseini, and Y. S. Zhang, "Coaxial extrusion bioprinting of 3D microfibrous constructs with cell-favorable gelatin methacryloyl microenvironments," *Biofabrication,* vol. 10, no. 2, p. 024102, 2018/01/12 2018, doi: 10.1088/1758-5090/aa9d44.

[70] A. V. da Silva, S. A. Gouvea, A. P. da Silva, S. Bortolon, A. N. Rodrigues, G. R. Abreu, and F. L. Herkenhoff, "Changes in retinal microvascular diameter in patients with diabetes," *Int J Gen Med,* vol. 8, pp. 267-73, 2015, doi: 10.2147/IJGM.S83749.

[71] H. J. Kuo, C. L. Maslen, D. R. Keene, and R. W. Glanville, "Type VI collagen anchors endothelial basement membranes by interacting with type IV collagen," *J Biol Chem,* vol. 272, no. 42, pp. 26522-9, Oct 17 1997, doi: 10.1074/jbc.272.42.26522.

[72] N. L'Heureux, S. Paquet, R. Labbe, L. Germain, and F. A. Auger, "A completely biological tissue-engineered human blood vessel," *FASEB J,* vol. 12, no. 1, pp. 47-56, Jan 1998, doi: 10.1096/fasebj.12.1.47.

[73] D. Oh, S. Lee, K.-I. Koo, and J.-M. Seo, "Microscopic Tubular Cell Organization for Artificial Vascularization," Cham, 2015: Springer International Publishing, in 6th European Conference of the International Federation for Medical and Biological Engineering, pp. 322-325.

[74] D.-H. T. Nguyen, S. C. Stapleton, M. T. Yang, S. S. Cha, C. K. Choi, P. A. Galie, and C. S. Chen, "Biomimetic model to reconstitute angiogenic sprouting morphogenesis in vitro," *Proceedings of the National Academy of Sciences,* vol. 110, no. 17, p. 6712, 2013, doi: 10.1073/pnas.1221526110.

[75] S. Kim, M. Chung, and N. L. Jeon, "Three-dimensional biomimetic model to reconstitute sprouting lymphangiogenesis in vitro," *Biomaterials,* vol. 78, pp. 115-128, 2016/02/01/ 2016, doi: 10.1016/j.biomaterials.2015.11.019.

[76] S. Kim, H. Lee, M. Chung, and N. L. Jeon, "Engineering of functional, perfusable 3D microvascular networks on a chip," *Lab on a Chip,* 10.1039/C3LC41320A vol. 13, no. 8, pp. 1489-1500, 2013, doi: 10.1039/C3LC41320A.

[77] S. Noria, F. Xu, S. L. McCue, M. E. Jones, A. I. Gotlieb, and B. L. Langille, "Assembly and reorientation of stress fibers drives morphological changes to endothelial cells exposed to shear stress," *The American journal of pathology,* vol. 164 4, pp. 1211-23, 2004.

[78] K. Nagayama and T. Matsumoto, "Contribution of actin filaments and microtubules to quasi-in situ tensile properties and internal force balance of cultured smooth muscle cells on a substrate," *American Journal of Physiology-Cell Physiology,* vol. 295, no. 6, pp. C1569-C1578, 2008/12/01 2008, doi: 10.1152/ajpcell.00098.2008.

[79] A. Tan, K. Fujisawa, Y. Yukawa, and Y. T. Matsunaga, "Bottom-up fabrication of artery-mimicking tubular co-cultures in collagen-based microchannel scaffolds," *Biomater Sci,* vol. 4, no. 10, pp. 1503-14, Oct 20 2016, doi: 10.1039/c6bm00340k.

[80] N. C. f. B. Information. "PECAM1 platelet and endothelial cell adhesion molecule 1 [Homo sapiens (human)]." https://www.ncbi.nlm.nih.gov/gene?Db=gene&Cmd=ShowDetailView&TermToSearch=5175 (accessed 2019).

[81] K. Tardif, V. Hertig, C. Dumais, L. Villeneuve, L. Perrault, J.-F. Tanguay, and A. Calderone, "Nestin downregulation in rat vascular smooth muscle cells represents an early marker of vascular disease in experimental type I diabetes," *Cardiovascular Diabetology,* vol. 13, no. 1, p. 119, 2014/08/21 2014, doi: 10.1186/s12933-014-0119-6.

[82] S. Kim, M. Chung, J. Ahn, S. Lee, and N. L. Jeon, "Interstitial flow regulates the angiogenic response and phenotype of endothelial cells in a 3D culture model," *Lab on a Chip,* 10.1039/C6LC00910G vol. 16, no. 21, pp. 4189-4199, 2016, doi: 10.1039/C6LC00910G.

[83] J. H. Yeon, H. R. Ryu, M. Chung, Q. P. Hu, and N. L. Jeon, "In vitro formation and characterization of a perfusable three-dimensional tubular capillary network in microfluidic devices," *Lab on a Chip,* 10.1039/C2LC40131B vol. 12, no. 16, pp. 2815-2822, 2012, doi: 10.1039/C2LC40131B.

[84] N. C. f. B. Information. "ACTA1 actin alpha 1, skeletal muscle [Homo sapiens (human)]." https://www.ncbi.nlm.nih.gov/gene/58 (accessed 09/19, 2019).

[85] A. C. Dykes and G. L. Wright, "Down-regulation of calponin destabilizes actin cytoskeletal structure in A7r5 cells," *Can J Physiol Pharmacol,* vol. 85, no. 2, pp. 225-32, Feb 2007, doi: 10.1139/y07-005.

[86] J. D. Humphrey, "Blood Vessels, Mechanical and Physical Properties of," in *Encyclopedia of Materials: Science and Technology*, K. H. J. Buschow *et al.* Eds. Oxford: Elsevier, 2001, pp. 748-751.

[87] A. S. Bulick, D. J. Muñoz-Pinto, X. Qu, M. Mani, D. Cristancho, M. Urban, and M. S. Hahn, "Impact of Endothelial Cells and Mechanical

Conditioning on Smooth Muscle Cell Extracellular Matrix Production and Differentiation," *Tissue Engineering Part A,* vol. 15, no. 4, pp. 815-825, 2009/04/01, doi: 10.1089/ten.tea.2008.0179.

[88] H. Onoe, T. Okitsu, A. Itou, M. Kato-Negishi, R. Gojo, D. Kiriya, K. Sato, S. Miura, S. Iwanaga, K. Kuribayashi-Shigetomi, Y. T. Matsunaga, Y. Shimoyama, and S. Takeuchi, "Metre-long cell-laden microfibres exhibit tissue morphologies and functions," *Nature Materials,* vol. 12, no. 6, pp. 584-590, 2013, doi: 10.1038/nmat3606.

Appendices

Appendix A: Credits & Copyright Permissions

Notes on Copyright Licenses for Reproduction of Text and Figures in this Dissertation

Chapter 1:

For reproducing those figures that appeared in the following publication with credit to other sources, permission has also been sought from the respective sources.

Chapter 2

The text excerpts and the figures presented in Chapter Two are reproduced with permission from the following article:

D. Van Thuy, D. Thao Thi, C. Hwang Ho, B. Sung Hoon, and K. Kyo-in, "Coaxial printing of double-layered and free-standing blood vessel analogues without ultraviolet illumination for high-volume vascularised tissue," Biofabrication, 2020, DOI: 10.1088/1758-5090/abafc6.

Appendix B: Mechanical strength measurement for Chapter Two

To investigate mechanical strength of tubular scaffolds at time points, we manually designed a device to estimate stress-strain curves, breaking points based on a method which was reported by Onoe, *et al.* [88]. Briefly, the device consisted of one stretchable wire (piano wire - 500 µm diameter or glass capillary – 120 µm diameter, 5 cm length), a motile capillary (glass capillary, 1000 µm width, 5 cm length) (Figure 21). The stretchable wire was fixed at the end by gluing to PDMS block while the motile capillary was connected to a syringe pump which allows to move regularly during the measuring. Prior to the measuring, a tubular scaffold was glued to two points nearby the end of the stretchable wire and the motile capillary.

The force applying to the scaffold (F) was calculated as $F = k \times \Delta x$, where k is the spring constant while Δx is the deformation of the stretchable wire. The k was manually calculated to be 3.6 (N/m) for the piano wire or 0.006 (N/m) for the glass capillary according the deformation of the stretchable wire caused by the gravity force. The Δx was obtained by analysing videos which were captured by a webcam (C920 HD PRO WEBCAM, Logitech, U.S.A). The change in the length of the scaffold (ΔL) was calculated by $\Delta L = l - \Delta x$, where the l was the traveling distance of the moving glass capillary.

We measured six different types of single-layered cell-laden tubular scaffolds: Cell-free-D1-DW (cell-free scaffold in DI water at day 1), Cell-free-D2-DW (cell-free scaffold in DI water at day 2), Cell-free-D1-M (cell-free scaffold in cell culture media at day 1), Cell-free-D2-M (cell-free scaffold in cell culture media at day 2), Cell-D1-M (cell scaffold in cell culture media at day 1), Cell-D13-M (cell scaffold in cell culture media at day 13). Figure 21c shows typical stress-strain curves. Evidently, there is no significant difference in mechanical property between Cell-free-D1-DW and Cell-free-D2-DW (Figure 21c-d). However, the Cell-free-D2-M became considerably weaker than Cell-

free-D1-M when we compared the typical strain-stress curves and breaking points (*** $p < 0.001$). These results indicated that the cell culture media caused the scaffolds to be softer. In addition, the presence of NIH/3T3 at 0.8×10^6 cells/mL in the scaffolds reduced mechanical strength of the scaffold at even day 1 (*** $p < 0.001$). At day 13, cell scaffolds were broken when applied a force of 0.0083 N as the stress this was significantly different to that of Cell-D1-M scaffold. These results indicated that the cell culture media and the cell proliferation reduced the durability of alginate scaffolds.

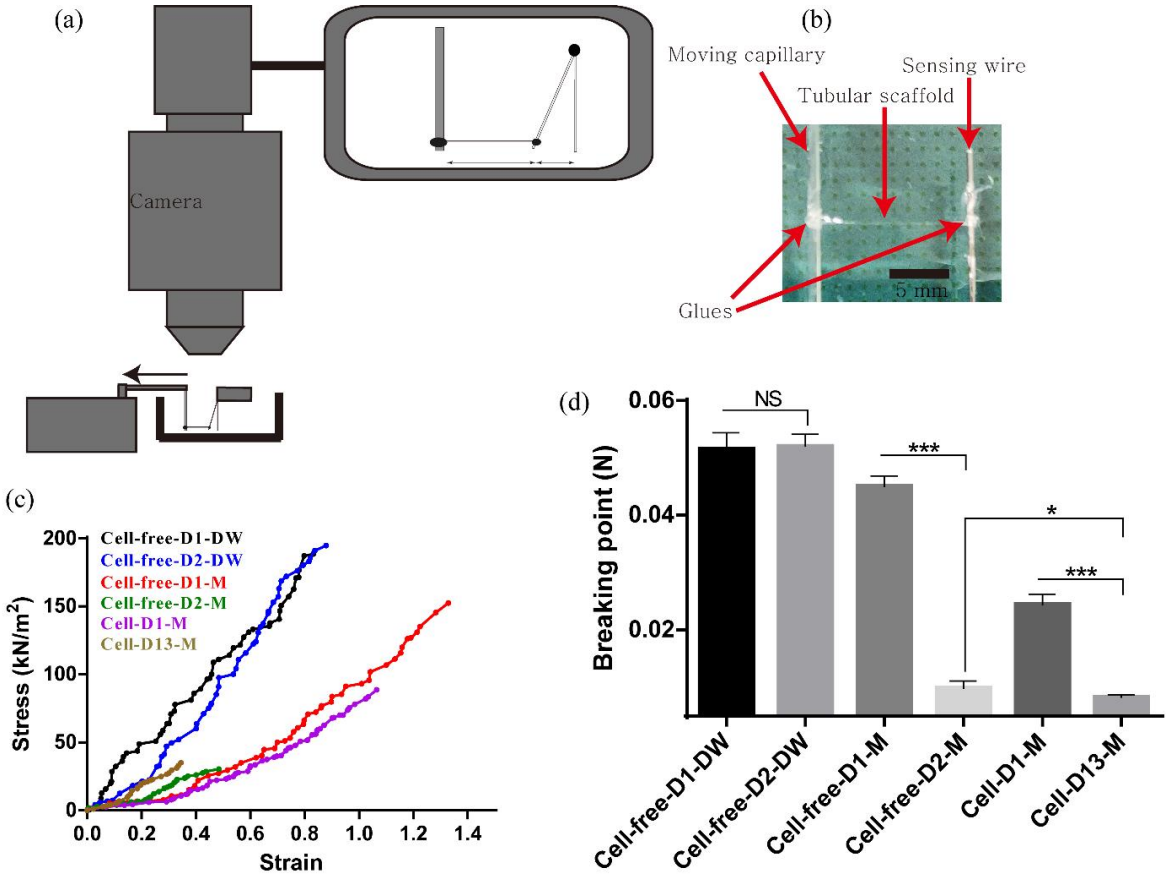

Figure 21: Mechanical strength measurement for microscopic tubular scaffolds. (a) The conceptual description of the mechanical strength measuring system. (b) The magnification of the sensing wire, the moving capillary, and the fixed scaffold. (c) The typical stress-strain curves. (d) The comparison of breaking points.